

2011

Stress Corrosion Cracking Evaluation of Candidate High Strength Stainless Steels for Prestressed Concrete

Joseph Rogelio Fernandez
University of South Florida, jfernandez@mail.usf.edu

Follow this and additional works at: <http://scholarcommons.usf.edu/etd>

 Part of the [American Studies Commons](#), and the [Materials Science and Engineering Commons](#)

Scholar Commons Citation

Fernandez, Joseph Rogelio, "Stress Corrosion Cracking Evaluation of Candidate High Strength Stainless Steels for Prestressed Concrete" (2011). *Graduate Theses and Dissertations*.
<http://scholarcommons.usf.edu/etd/3102>

This Thesis is brought to you for free and open access by the Graduate School at Scholar Commons. It has been accepted for inclusion in Graduate Theses and Dissertations by an authorized administrator of Scholar Commons. For more information, please contact scholarcommons@usf.edu.

Stress Corrosion Cracking Evaluation of Candidate High Strength Stainless Steels for
Prestressed Concrete

by

Joseph Fernandez

A thesis submitted in partial fulfillment
of the requirements for the degree of
Master of Science
in Materials Science and Engineering
Department of Mechanical Engineering
College of Engineering
University of South Florida

Major Professor: Alberto Sagüés, Ph.D.
Ashok Kumar, Ph.D.
Gray Mullins, Ph.D.

Date of Approval:
November 1, 2011

Keywords: 316L, XM29, 2205, Magnesium Chloride, Relative Humidity

Copyright © 2011 Joseph Fernandez

Acknowledgments

This work was supported by the Florida Department of Transportation. The opinions, findings, and conclusions expressed in this publication are those of the author and not necessarily those of the State of Florida Department of Transportation.

Table of Contents

List of Tables	ii
List of Figures	iii
Abstract	vi
Chapter 1: Introduction	1
1.1 Project Scope	1
1.2 Concrete and Steel	2
1.3 Corrosion and Passivation	8
1.4 Stress Corrosion Cracking	12
1.5 Literature Review	16
1.6 Preliminary Experiments	18
1.7 Objectives	19
1.8 Approach.....	20
Chapter 2: Methodology	22
2.1 Material Data	22
2.2 Specimen Preparations and Setup for Phase 1	24
2.3 Specimen Preparation and Setup for Phase 2	31
2.4 Insulating Enclosure and Tank Setup	36
Chapter 3: Results	45
3.1 Phase 1 Results	45
3.2 Phase 2 Results	59
Chapter 4: Overall Discussion	64
Chapter 5: Conclusions	66
Chapter 6: Future Work	68
References	69
About the Author.....	End Page

List of Tables

Table 1 Typical Composition and PREN Values of Stainless Steel Alloys (All Fe-Based).....	7
Table 2 Equilibrium Relative Humidities for Salts at Various Temperatures	29
Table 3 Temperature versus Absolute Pressure of Water and the Relative Humidity for that Case.....	30
Table 4 Temperature and Pressure of the Water at the Bottom of the Enclosure so that the Equilibrium Relative Humidity of MgCl is Equal to or Greater than the Relative Humidity at that Temperature and Pressure.	30
Table 5 Springback Amount for Each Alloy (in mm/ inches)	35
Table 6 Desired Base Solution Composition for 15 wt% Cl and SPS Solution (Table 3 [34])	39
Table 7 Results of Phase 1 Experiment Using MgCl ₂ and Pure Water X: Cracking; O: No Crack	49

List of Figures

Figure 1 Potential versus Current Density for Anodic - Cathodic Reaction with Passivation	10
Figure 2 Pourbaix Diagram of Iron (Fe) [11]	11
Figure 3 Stress Corrosion Crack Growth Rate as a Function of Tensile Yield Strength [14]	13
Figure 4 Photo of Supplied 316L Material	23
Figure 5 Photo of Supplied XM 29 Material	23
Figure 6 Photo of Supplied 2205 Material.....	24
Figure 7a Bending Frame, Test Assembly, and Heater	25
Figure 7b Diagram of Bending Frame	25
Figure 8a Phase 1 Test Enclosure	28
Figure 8b Diagram with Test Setup Process Parameters	28
Figure 9 Bending Jig with 316L Specimen.....	32
Figure 10a Bent 316L Specimen (1sq =1 mm).....	33
Figure 10b Relaxed 316L Specimen (1sq =1 mm).....	33
Figure 10c Bent XM 29 Specimen (1sq =1 mm).....	34
Figure 10d Relaxed XM 29 Specimen (1sq =1 mm).....	34
Figure 10e Bent 2205 Specimen (1sq =1 mm)	35
Figure 10f Relaxed 2205 Specimen (1sq =1 mm)	35
Figure 11a Phase 2 Test Enclosure	41

Figure 11b U-Bend Specimen Dimensions.....	42
Figure 11c Diagram of Overall Insulated Tank Setup	43
Figure 12 Process Controller and Wiring Setup for Second Test.....	44
Figure 13 Specimen A1 316L @135°C (275 °F) Cracked after 48 Hours.....	50
Figure 14 Specimen A2 316L @ 135°C (275 °F) Cracked after 4 Hours.....	51
Figure 15 Specimen A3 316L @ 135°C (275 °F) Cracked after 1 Hour	51
Figure 16 Specimen A4 316L@ 90°C (194 °F) Cracked after 96 Hours.....	52
Figure 17 Specimen A5 316L @90°C (194 °F) Cracked after 48 Hours.....	52
Figure 18 Specimen A6 316L @90°C (194 °F) Cracked after 24 Hours.....	53
Figure 19 Specimen A7 316L @90°C (194 °F) Cracked after 4 Hours.....	53
Figure 20 Specimen A9 316L @60°C (140 °F) Cracked after 168 Hours.....	54
Figure 21 Specimen A12 316L @60°C (140 °F) Cracked after 96 Hours.....	54
Figure 22 Specimen B1 XM 29 @ 135°C (275 °F) Cracked after 48 Hours.....	55
Figure 23 Specimen B3 XM29 @135°C (275 °F) Cracked after 24 Hours	55
Figure 24 Specimen C4 2205 @135°C (275 °F) Cracked after 24 Hours	56
Figure 25 Specimen C5 2205 @135°C (275 °F) Cracked after 4 Hours	56
Figure 26 Specimen C6 2205 @135°C (275 °F) Cracked after 1 Hour	57
Figure 27 Specimen C9 2205 @90°C (194 °F) Cracked after 96 Hours	57
Figure 28 Graph of Exposure Time (Log Scale) Indicating Test Outcome, as Function of Inverse Absolute Temperature.	58
Figure 29 Potential versus Time for 316L Specimens #1 through #6 (SCE versus ATR)	61
Figure 30 Potential versus Time for XM29 Specimens #7 through #12 (SCE versus ATR)	62

Figure 31 Potential versus Time for 2205 Specimens #13 through #18 (SCE
versus ATR) 63

Abstract

Prestressed concrete piles are commonly used to support over-water highway bridges in marine environments. The reinforcing steel within will ultimately be degraded via corrosion damage due to the penetration of chloride ions from sea water. The service life of these structures is, in part, dictated by the time required to diffuse chloride ions through the concrete cover and subsequently corrode the steel. Therefore, by slowing the rate of diffusion or increasing the chloride threshold of the steel (or both) an increased service life can be expected. This thesis focuses on the latter whereby stainless steel reinforcing alternatives were investigated to elevate the chloride threshold before corrosion begins.

The designation “stainless” steel implies corrosion resistance. However, corrosion resistance in itself is not a sufficient condition to make it a suitable alternative for prestressed concrete applications. In this study, the corrosion susceptibility of stainless steel alloys was scrutinized with the understanding that high strength stainless steels are vulnerable to stress corrosion cracking (SCC). This investigation screened three candidate alloys that span the norms of stainless steel compositions: a common austenitic stainless steel with high nickel content (316L), a less common austenitic stainless steel with low nickel but high manganese (XM 29), and a duplex stainless steel with high chromium and an additional constituent, molybdenum (2205). Each alloy was subjected to two stress conditions imposed by varied mechanical fixtures then subjected to various

forms of high chloride concentrations. The pH of these conditions was also varied and in one case simulated the high pH common to concrete pore water solutions. Elevated temperatures were used to accelerate the effects of these exposures.

Results of Phase 1 showed that for exposure at 135°C (275°F) cracking of alloys 316 L and 2205 occurred after 1 hour while XM29 experience cracking after 24 hours. At 90°C (194°F) alloy 316L cracked after 4 hours; XM29 did not crack after 96 hours while 2205 did crack after 96 hours. The results were interpreted with an Arrhenius relationship between time to cracking and test temperature to extrapolate toward the anticipated service regime. Results of Phase 2 showed that SCC was less likely to initiate in high pH conditions than in low pH conditions at typical marine environment temperatures and chloride concentration. In these limited tests the SCC performance of XM29 was better relative to that of the other two alloys.

Chapter 1: Introduction

1.1 Project Scope

In Florida, the durability of ground travel infrastructure is a key issue both economically and in engineering. An ambitious durability goal of a service life of 75 years for bridges has been set by the Florida Department of Transportation [1]. The areas of the bridge most affected by factors that can reduce the durability of the structure are the bridge piles.

Bridge piles can be made with carbon steel reinforcement bar (e.g. rebar) or prestressed with carbon steel strands and encased within concrete. Prestressed bridge piles are commonly used and made by pouring concrete over tensioned high strength strands placed in the mold, and releasing the tension on those strands after the concrete has reached sufficient strength. The release of tension on the strands imposes a compressive force onto the concrete, which in turn gives the concrete an apparent tensile strength [2]. One of the main issues that limit the durability of prestressed bridge piles and other road construction is corrosion of the strands.

A solution to the issue of corrosion of carbon steel in prestressed concrete is to use stainless steel as the prestressed material. Stainless steel costs more to use than carbon steel (see the next section for the discussion of cost), but the overall intrinsic corrosion resistance of stainless steel promises to outweigh the cost penalty. However, a

potential problem with stainless steels processed to obtain high-strength is their increased susceptibility to a particular form of localized corrosion called Stress Corrosion Cracking (SCC). The main question considered by this study is: “For prestressed construction of concrete bridge piles in the average Florida marine environment, is SCC susceptibility be enough of a concern to affect the suitability of high-strength stainless steel to achieve a service life goal of 75 years?”

1.2 Concrete and Steel

Concrete has good compression strength (e.g. 17-70 MPa/ 2.5-10 ksi), but a poor tensile strength (e.g. 1-7 MPa/ 0.2-1 ksi) [3,4], and therefore needs an embedded material with good tensile strength (and preferably high ductility) to act as a reinforcement and create a composite material with appropriate overall performance. The use of reinforcement bar (rebar) is the most common method of giving tensile strength to concrete structures without losing the properties (ex: high compression strength, low cost of material, etc.) of concrete favored in reinforced construction. The steel rebar must be of high tensile strength, as it must be able to hold the loads applied to the structure, with a significant factor of safety. Since at least 1880, carbon steel has been used as the material for rebar in all manner of construction projects (ex: buildings, bridges, roads, barriers and many other construction projects) [5]. Its high tensile strength (e.g. 414 MPa/ 60 ksi) [6] and good availability have been instrumental in making carbon steel the choice for that application. For prestressed concrete, even higher strength material (e.g. 1.86 GPa/ 270 ksi) [6] is needed for the strands. The alloy used is again carbon steel, typically of eutectoid composition and highly cold worked. It has only been in the last decade or so

that stainless steels have been frequently considered and increasingly used by engineers as rebar material in concrete construction. More recently, the use of high-strength stainless steels have been considered for use as prestressing strand.

Stainless steels are iron-base alloys that contain at least 11% Chromium (the amount needed in the alloy to prevent active corrosion from occurring) which is what makes it “stainless”. For the application as a structural material in marine environments, under large loads and corrosive environments, only certain stainless steel alloys may be viable.

There are four families of stainless steels: Ferritic, Martensitic, Austenitic, and Duplex. Precipitation Hardening stainless steels are a separate category as rather than a change in microstructure, it is a change in the heat treatment process that classifies them. The first family of stainless steels is the Ferritic family. Ferritic stainless steels start at the base form 405 (UNS S40500) to which more Chromium is added going from 14.5% to 18% to make 430 (UNS S43000). From there, even more Chromium is added, up to 30%, to make 442 (UNS S44200). Ferritic stainless steels do not have enough pitting corrosion resistance to be used in marine environments as well as having a lower strength than the strength required for strands. Ferritic stainless steel is also magnetic, with poor toughness and weldability.

The second family of stainless steels is the Martensitic family. The Martensitic stainless steels start at the base form of 403 (UNS S40300) to which more Chromium is added going from 11% to 14% and Carbon going from 0.15% to 0.3% to make 420 (UNS S42000). From there, even more Chromium and Carbon are added, up to 18% and 1.2% respectively, to make 440C (UNS S44004). Carbon is added to add hardness to the alloy.

Martensitic stainless steels are very strong and hard but are not ductile enough for use in a high strength environment, such as reinforcing bars for concrete.

The third family of stainless steels is the Austenitic family. The austenitic (Face Centered Cubic, or FCC) microstructure is inherently more ductile than either the ferritic or martensitic (body centered cubic, or BCC and body centered tetragonal, or BCT respectively) microstructure, and this difference in microstructure is achieved by the addition of α -phase (austenitic) stabilizing elements such as Nickel as well as Manganese and Nitrogen. At room temperature iron has a stable BCC microstructure, so to maintain austenitic steels in the FCC microstructure; elements must be added to stabilize the unstable FCC microstructure, these elements are referred to as austenitic phase stabilizers. This family of stainless steel is the most expansive and diverse of the four families of stainless steels. Austenitic stainless steels can be divided up into two sub-families of stainless steel: Chromium-Nickel alloys and Chromium-Manganese-Nitrogen. The Austenitic stainless steel sub-family of Chromium-Nickel alloys start at the base form of 301 (UNS S30100) to which more Chromium, from 18% to 20%, Nickel, from 8% to 12%, and less Carbon, from 0.15% to 0.03% is added to make 304L (UNS S30403). From there, less Chromium is used, down to 18%, but more Nickel and Molybdenum is added, up to 14% and 3% respectively, to make 316L (UNS S31603). Molybdenum is added to stainless steel to increase the pitting corrosion resistance of the steel as well as the general corrosion resistance in chloride environments.

The Austenitic stainless steel sub-family of Chromium-Manganese-Nitrogen alloys start at the base form of 201 (UNS S20100) to which more Manganese, from 7.5% to 9% is added to make Nitronic 60 (UNS S21800). From there, less Chromium is used

and much less Carbon is used, down to 17% and 0.03% respectively, but Nitrogen is added, up to 0.3%, to make XM 29 (UNS S24000).

The fourth family of stainless steels is the Duplex family. The Duplex family start at the base form of 329 (UNS S32900) to which less Chromium and Carbon are used, from 28% to 23% and 0.2 to 0.03 respectively, but more Nickel, from 5% to 6.5%, Molybdenum, from 2% to 3.5%, and Nitrogen, from ~0% to 0.2% are added to make 2205 (UNS S31803). Duplex stainless steels are a balance of Austenitic and Ferritic stainless steel properties (Duplex stainless steel is a mixture of both austenitic and ferritic phases). This combination helps give Duplex stainless steels resistance to stress-corrosion cracking and improved ductility and toughness when compared to just Austenitic or Ferritic stainless steels while also having the general corrosion resistance that Austenitic stainless steel has.

Precipitation Hardened Stainless Steels are Chromium-Nickel alloys which can be age hardened. Age hardening is the process of a material growing in hardness and strength due to reactions of certain elements into the alloy over time. Some examples of elements that are alloyed into Precipitation-Hardened stainless steels are Copper, Titanium, Aluminum, and Niobium. Precipitation Hardened stainless steels have high yield strengths like Martensitic stainless steels due to the precipitation hardening. While they do have good ductility and toughness, they are still too hard and not ductile enough for use as strands.

A table of elemental compositions for the stainless steels mentioned above is listed in Table 1 [7]. The Pitting Resistance Equivalent Number (PREN) is a merit figure that describes the relative pitting corrosion resistance of an alloy based on its elemental

compositions. “The PREN is calculated by adding the weight percentages of elements that affect pitting corrosion resistance—namely, Chromium, Molybdenum, and Nitrogen—and then normalizing them with respect to the effect of 1% Chromium.”[7] The calculation used to obtain the values in Table 1 was $\% \text{Cr} + 3.3 * \% \text{Mo} + 16 * \% \text{N}$.

Phosphorous and Sulfur content of an alloy can have a negative effect on the PREN number, but this negative effect is not significant for comparison between the alloys listed as their Phosphorous and Sulfur contents are very similar.

The relative cost of the stainless steel alloys as compared to carbon steel as well as to each other is another factor in the selection process. There is a considerable increase in the cost of the material when going from carbon steel to stainless steels. Carbon steel costs about \$0.80 per kilogram versus 316L stainless steel which costs \$3.68 per kilogram. XM 29 is the least expensive of the three stainless steels considered at \$2.69 per kilogram, while 316L is most costly, and 2205 falls in the middle cost-wise at \$3.06 per kilogram [8].

The major factor in the higher cost of stainless steel as compared to carbon steel is the cost of the alloying elements put into the stainless steel. Nickel-austenitic alloys such as 316L are expensive compared to some other stainless steels due to the high price of Nickel. Manganese is a much less expensive substitute for Nickel to achieve an austenitic structure and brings down the cost of alloy XM 29. The cost of Molybdenum is also high, which is an added factor in the higher cost of alloy 316L as well as of some duplex steels such as alloy 2205. Therefore, all benefits of better corrosion resistance and the resulting longer life span must be weighed against the increase of cost in construction that will occur if stainless steels are used in place of carbon steel.

One possibility to reduce this cost increase is to only use the stainless steel in the parts of the construction closest to the seawater (e.g. using stainless steel only in the piles of a bridge and not in the upper structure of the bridge).

**Table 1 Typical Composition and PREN Values of Stainless Steel Alloys
(All Fe-Based)**

Alloy	% Cr	% Ni	% Mo	% N	% Mn	% C	%S	%P	%Cu	%Si	PREN
405	14.5	-	-	-	1	0.08	0.03	0.04	-	1	14.5
430	18	-	-	-	1	0.12	0.03	0.04	-	1	18
442	30	-	-	-	1	0.2	0.03	0.04	-	1	30
403	11	-	-	-	1	0.15	0.03	0.04	-	0.5	11
420	14	-	-	-	1	0.3	0.03	0.04	-	1	14
440C	18	-	0.75	-	1	1.2	0.03	0.04	-	1	20.48
301	18	8	-	-	2	0.15	0.03	0.05	-	1	18
304L	20	12	-	-	2	0.03	0.03	0.05	-	1	20
316L	18	14	3	-	2	0.03	0.03	0.05	-	1	27.9
201	18	5.5	-	0.25	7.5	0.15	0.03	0.06	-	1	22
Nitronic 60	18	9	-	0.2	9	0.1	0.03	0.04	-	4.5	21.2
XM29	17	3	-	0.3	9	0.03	-	-	1	1	21.8
329	28	5	2	-	1	0.2	0.03	0.04	-	0.75	34.6
2205	23	6.5	3.5	0.20	2	0.03	0.02	0.03	-	1	37.8

Three stainless steels were chosen based on the present availability of the materials in their high strength form, as well as good corrosion resistance needed for a marine environment. The three alloys are: 316L, XM29 and 2205.

1.3 Corrosion and Passivation

Typically, corrosion is considered to be the deterioration of a metal as a result of an electrochemical reaction with the environment (electrolyte). Corrosion requires four components: the anodic reaction (which is the actual corrosion event (metal dissolution)), the cathodic reaction (which consumes the electrons produced by the anodic reaction), the medium (electrolyte), and an electronic path.

As metal dissolves in the form of ions into the solution, electrons are left behind. In the absence of a cathodic reaction, the accumulation of electrons would hinder further metal dissolution, which is why the cathodic reaction is an integral part of the corrosion process.

Below are typical anodic and cathodic reactions for the dissolution of iron in cementitious systems where the liquid medium is highly alkaline:

$\text{Fe} \rightarrow \text{Fe}^{2+} + 2\text{e}^-$, which is the anodic (oxidation) reaction and

$\text{O}_2 + 2\text{H}_2\text{O} + 4\text{e}^- \rightarrow 4\text{OH}^-$, which is the cathodic (reduction) reaction.

The rate of the anodic reaction increases if the potential of the metal with respect to the medium (electrolyte) becomes more positive. In contrast, the rate of the cathodic reaction increases as the potential becomes more negative. Consequently, the system reaches a steady state condition at some intermediate potential (the corrosion potential) where the rate of both the anodic reaction and the cathodic reaction are the same. This is the basis of the Mixed Potential Theory [9].

Under certain conditions, carbon steel forms a highly protective layer (called a passive film) which provides a barrier that hinders the anodic reaction. “In normal Portland cement concrete made with uncontaminated water and nonaggressive

admixtures or aggregates, the pore water solution contains mostly K^+ , Na^+ , Ca^{++} , and OH^- ions (typically $12.5 < pH < 13.5$), and dissolved O_2 from atmospheric exposure. Under those conditions, the steel of a reinforcing bar (rebar) and other carbon steel components embedded in concrete is in the passive condition, with effective corrosion rates $\ll 1 \mu m/y$.”[10]

Figure 1 shows a generic potential versus log anodic current density graph [9] for a metal that exhibits passive behavior. The region encircled in red indicates the passive region. At potentials lower than this passive region the metal corrodes. This is known as the active condition (anodic current density increases exponentially with potential). Once a critical passivation potential is reached, $E_{passive}$, (illustrated in Figure 1 as a dotted line from the anodic curve to the y-axis) the passive film forms and the anodic reaction rate decreases dramatically.

For the case of a metal exposed to an oxidizing species the system reaches steady state at the corrosion potential designated as $E_{passive}$. This is the intersection between the anodic and cathodic curves. In Figure 1 $E_{passive}$ falls in the passive regime. The associated current density, known as $i_{passive}$ (indicated by a dotted line from the anodic curve to the x-axis) is low. Since the current density is directly related to the corrosion rate, the corrosion rate is also low for a metal in a passive state.

If the passive film breaks down the metal remains in the active condition over a wide potential range as indicated by the dashed line in Figure 1. Consequently, for the active condition, the intersection with the cathodic reaction line occurs at a lower potential E_{active} (indicated by a dotted line from the cathodic curve to the y-axis) and typically a much higher current density i_{active} (indicated by a dotted line from the cathodic

curve to the x-axis) than in the passive case. Because a drop in potential relates to an increase in current density, the measurement of the potential of a metal can be an indicator of its corrosion state. The Open Circuit Potential (OCP) of a metal can be measured. A sudden and significant lowering of potential can indicate the onset of passive film breakdown.

This indication of passive film breakdown may be a symptom of pitting corrosion or SCC because involves the breakdown of passive films [9]. Pitting corrosion can also lead to SCC.

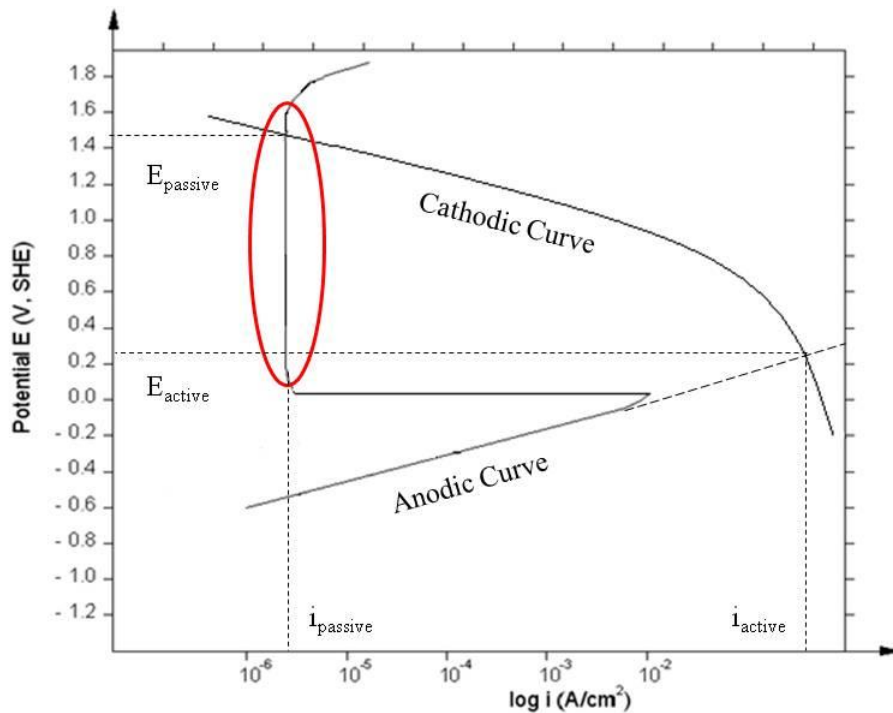


Figure 1 Potential versus Current Density for Anodic - Cathodic Reaction with Passivation

Thermodynamic models, plotted in the form of Pourbaix Diagrams [11], were used to determine the regimes where the passive films of different materials are stable. These diagrams correlate the electrical potential of the metals with the pH of the electrolyte.

In the case of Iron in water at 25°C, different soluble or insoluble corrosion products are produced depending on the pH and the electrical potential. Soluble products for iron include Fe^{++} , Fe^{+++} , and HFeO_2^- . Insoluble products for iron include $\text{Fe}(\text{OH})_2$, Fe_2O_3 , and Fe_3O_4 . [11]

The passive, immune, and active regions for Fe (generally applicable to plain carbon steel which is mostly Fe) are shown in Figure 2. The passive region of the diagram is where the insoluble products are sufficiently adherent and impermeable that corrosion of the underlying metal is essentially stifled. [11]

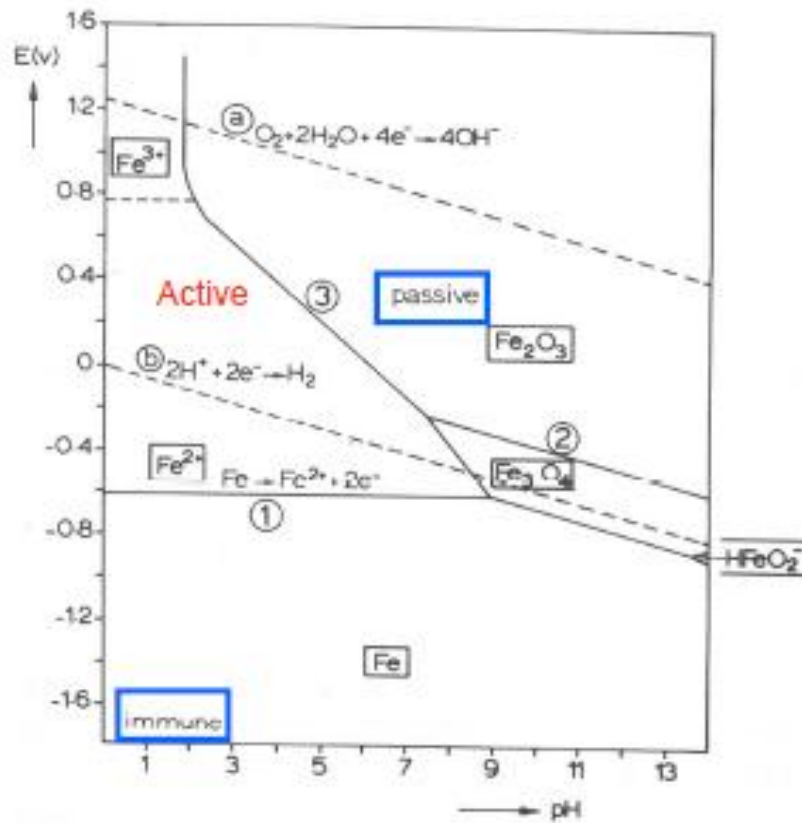


Figure 2 Pourbaix Diagram of Iron (Fe) [11]

Normal environmental conditions for Tampa, Florida consist of relative humidity ranging between 52 % and 91%, and temperature ranging between 11°C and 32°C (per National Oceanic and Atmospheric Administration data for Tampa, FL). As indicated

earlier concrete pore water (the electrolyte) typically has a high pH. This combination of environmental conditions is not normally considered to be conducive to SCC in stainless steels [12 and 13]. The environmental conditions of above-average temperatures, lower pH, and higher relative humidity are conducive to SCC, and are discussed below.

1.4 Stress Corrosion Cracking

When under stress and subject to corrosion, steel under some circumstances becomes more brittle and any preexisting cracks propagate more rapidly, or new cracks appear as well. This is a rudimentary description of the process of SCC. SCC requires three conditions to be met before it can occur. These are: an environment in which a corrosive agent exists, a material susceptible to the corrosive agent, and a material under a tensile stress. The risk is greater the greater the stress [9].

Figure 3 shows that there is a correlation between yield strength and SCC growth rate [14]. It is readily apparent there that high yield strength materials such as high-strength stainless steel present greater risk of SCC. This is in part because the highest elastic stress level that a material can support is in the order of its yield strength, so the risk of SCC increases accordingly. As Figure 3 shows, the increase turns out to be an exponential function of the yield strength. As indicated in the Introduction, strands used in prestressed construction have a yield strength (e.g. 1860 MPa) that is at about the high end of strength in the abscissa of Figure 3, while carbon steel rebar has a much lower yield strength (e.g. 414 MPa), even beneath the low end in the same axis. This ~5 factor difference in yield strength translates into a 10 million factor difference in expected SCC crack growth rate. That suggests that, while significant SCC might not have been

observed yet in stainless steel rebar applications (see Section 1.5), it could well be a severe problem when the stainless steels are strengthened to the levels required for prestressing strand service. This concern was a key issue in originating this investigation.

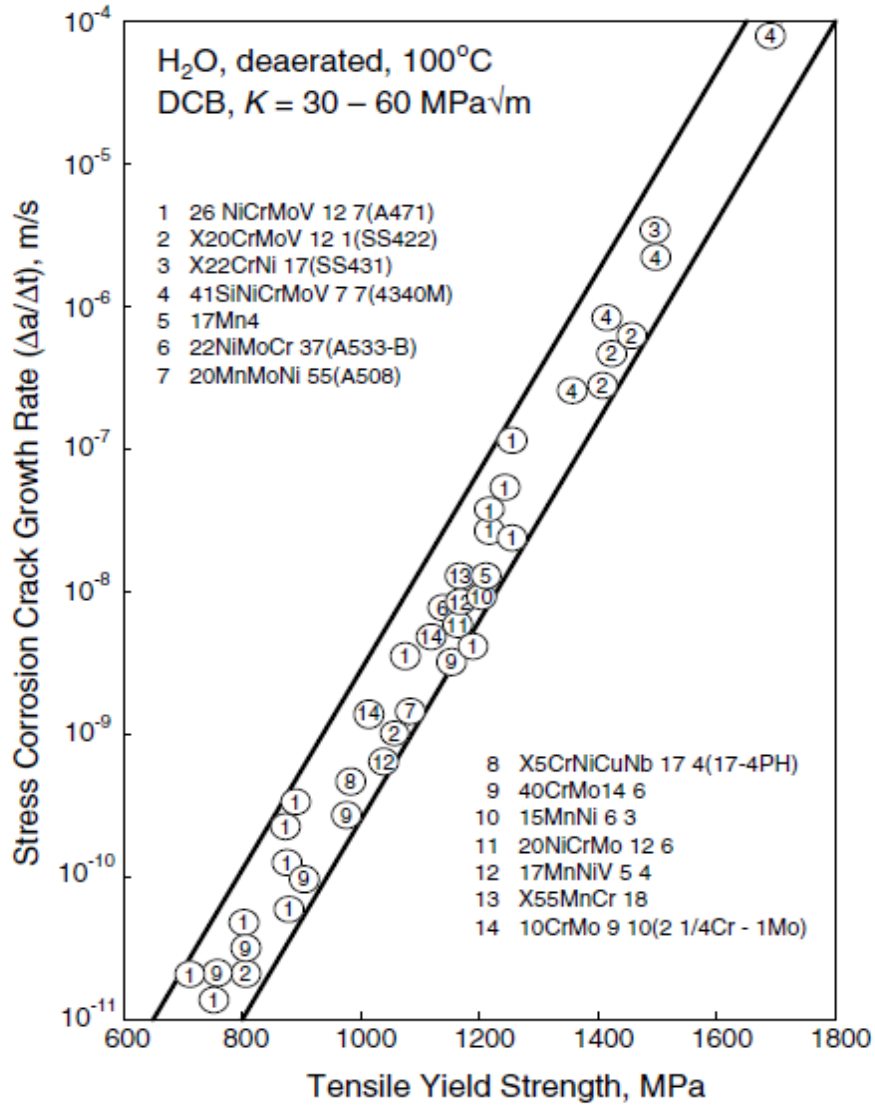


Figure 3 Stress Corrosion Crack Growth Rate as a Function of Tensile Yield Strength [14]

In a marine environment, the main corrosive agents are chloride ions, which come from seawater containing ~ 1M NaCl and smaller amounts of MgCl₂. Chloride ions diffuse through the concrete cover and upon reaching the embedded steel in sufficient quantity, begin passive film breakdown.

The stress placed on the strands results from the construction procedure used to create prestressed concrete as well as the loads of the structure.

SCC results in brittle failures, which are best addressed in terms of Fracture Mechanics concepts. An important concept in Fracture Mechanics is Stress Concentration, whereby the stress at elastic discontinuities can be much higher than at the bulk region. The tip of a crack in the material is an example of a stress concentration location.

The ratio of the stress, σ_m , on the material at the stress concentration location to the applied (bulk) stress on the material, σ_0 , is called the Stress Concentration Factor. The stress concentration factor is simply a measure of the degree to which an external stress is amplified at the tip of a crack. Linear elastic mechanics calculations show that the stress concentration factor is given by:

$$K_t = \sigma_m / \sigma_0 = 2(a/\rho_t)^{1/2} \quad (\text{Equation 1})$$

where:

a is the length of the crack,

and ρ_t is the radius of curvature of the crack [15].

Per Equation 1, if a crack increases in length, the stress concentration increases too thus further promoting the growth of the crack. However, at the tip of the crack, dislocation motion at an angle to the sides of the crack causes the material at the crack tip

to deform from an idealized sharp “V” shape, into a blunt “U” shape. That increase in the radius of curvature of the crack tip, or blunting of the tip, causes the stress concentration factor to decrease per Equation 1. Depending on how pronounced this mitigating effect becomes compared with the aggravating effect of increasing the crack length, a crack could continue to propagate or not. The blunting effect depends on the mechanisms for plastic deformation of the material in question. A practical way of quantifying this issue for design purposes when selecting materials is to introduce a sharp crack of known length in the material, apply stress and observe at what stress level the crack begins to propagate. To that end a quantity has been defined called the Stress Intensity Factor, that captures the crack length effect. For the simple case of tensile stress perpendicular to the crack plane the quantity is

$$K=f\sigma(\pi a)^{1/2} \quad \text{(Equation 2)}$$

where:

K is the stress intensity factor,

f is a geometric factor for the specimen and crack,

σ is the applied stress,

and a is the crack size.[15]

Unlike the stress concentration factor, the stress intensity factor has no dependence on the radius of curvature of the crack. The value of K at which the crack begins to propagate is referred to as the Fracture Toughness, K_c , which is a property of the material. Fracture Toughness generally decreases as the thickness of the metallic piece increases, and tends for very thick sections to a limit value (worst case) which is called the Plane Strain Fracture Toughness, K_{IC} . As an example: for 4340 tempered steel,

the $K_{IC} = 45.8 \text{ ksi in}^{1/2}$ while the yield strength $\sigma_y = 238 \text{ ksi}$ [15]. Using Equation 2, the stress needed to reach $K_{IC} = 45.8 \text{ ksi in}^{1/2}$ for a crack of 1 inch in length is 21.53 ksi, which is much less than yield strength.

Thus if a preexisting crack in the material is of enough size, failure can occur at a stress much below the yield strength of the material. [15]

For SCC, there is also a critical stress intensity factor, lower than K_{IC} , that must be reached or exceeded for crack initiation and propagation. This lower stress intensity factor is known as K_{ICSCC} . For example, for 4340 steel hardened to 53 HCR at low strain rates K_{IC} is $\sim 14 \text{ ksi in}^{1/2}$ in distilled water, but K_{ISCC} is only $\sim 7 \text{ ksi in}^{1/2}$ in 3.5% NaCl solution where SCC is in effect.[16]

1.5 Literature Review

A literature review was performed to ascertain the current state of knowledge of SCC in High-Strength Stainless Steels for Prestressed Concrete for use in marine environments.

General aspects of SCC in stainless steel are well known and compilations of that data exist in the literature (Jones [17]).Hence, these aspects will not be further reviewed here.

SCC of high-strength carbon steel in concrete applications has been documented by Andrade [18]. In those studies, the corrosive agent was chloride ions. However, instances of undetermined causes have been noted as well by Valiente [19].

The literature has clearly established superior resistance to general corrosion by stainless steel in concrete as compared to that of carbon steel per Andersen and Sjong [5,20,21]. However, very little documented evidence exists about SCC of stainless steel in concrete, with the exception of one possible incident at Progresso Pier [5, 22], but in that case, the stainless steel bar was not in the concrete but instead was in the form of an externally exposed bent end hook. Consequently, further investigation is merited as to whether SCC can occur in stainless steel in concrete.

In particular, the question arises as to whether SCC is at all possible in the relatively low temperatures related to service in concrete structures (e.g. $< 40^{\circ}\text{C}$) [21]. In that context, it is noted that traditionally, SCC was not considered likely unless the temperature was greater than 100°C as stated by Fontana [9]. But in recent decades, increasing evidence has emerged of SCC at near ambient temperatures as noted by Oldfield [12]. Notably, a recent study by Prosek showed that SCC of alloy 316L could occur in temperatures as low as 30°C [23]. That study also revealed that duplex stainless steel, such as 2205, tended to have more SCC resistance than regular austenitic stainless steel as documented by Prosek and Bhattacharya [23, 24]. Other studies showed that alloys where Manganese was substituted for Nickel, such as XM 29, tended to have less corrosion resistance than regular austenitic stainless steel as documented by Toor and Devasenapathi [25, 26]). The thermal activation aspects of SCC, i.e. the relationship of SCC to temperature change, were documented by Lu and Alyousif [27, 28]. Those studies provide the basis for the extrapolation of results of high temperature SCC tests to lower temperatures.

In a recent investigation on producing high strength corrosion resistance strand for prestressed concrete Moser [29] conducted some preliminary evaluation of SCC susceptibility of stainless steels, using the slow strain rate test method. Alloys evaluated included 316L and 2205. The investigation consisted of tests in simulated concrete pore water solutions with Cl^- concentrations of 0.5 M. The slow strain rate tests showed that in alkaline and carbonated solutions at 24°C (75°F) with 0.5 M Cl^- , 2205 experienced no SCC, while 316L experienced pitting corrosion (which can lead to SCC) under those same conditions.

In conclusion, very little evidence of observations of SCC of stainless steel in concrete was uncovered by this review. The possibility of SCC in concrete being promoted by the high yield strength of stainless steel strand appears not to have received much attention. There was increasing evidence that SCC is possible at moderate temperatures of interest to concrete applications. These findings confirm the need for further investigation of the potential for SCC in high-strength stainless steels for use in prestressed concrete, which is addressed in this thesis.

1.6 Preliminary Experiments

An exploratory study had been conducted in this laboratory where 316L and XM29 strand wires were placed in a three-point bending frame, to apply stress at a center point whose distance from the outer points is fixed and known. The specimen and the frame were then submerged in a boiling saturated NaCl solution (106°C / 220°F). This preliminary study showed that XM29 would experience cracking (after 6 days) while

316L would not (after 90 days). It was noted that the frames for the XM29 were not corroded, while there was heavy corrosion on the frames for the 316L. This observation of frame corrosion was one of the driving forces for the set of experiments done in the research described in this thesis. It is believed that the results of the NaCl boiling test were altered due to the artifact of galvanic prevention given to the 316L by the corroding bending frames. Galvanic prevention occurs when two different metals are in contact with each other. The corrosion of the less corrosion-resistant metal causes the potential of other metal in contact to become more negative, thus making anodic processes such as SCC less likely. This cathodic prevention effect is an artifact that needed to be eliminated in continuation testing.

Therefore, the experiments described in this thesis aimed to establish the SCC performance of the candidate alloys were designed to eliminate any galvanic prevention from the frame or securing devices used.

The question of whether SCC can happen at near-ambient temperatures, noted in the literature review, was addressed by conducting tests at a range of temperatures including more moderate regimes (around 60°C or 140°F) and extrapolating to near-ambient temperature cases.

1.7 Objectives

The following summarizes the objectives of this research.

- Devise and implement an approach for evaluating susceptibility to SCC of candidate high-strength stainless steel alloys under accelerating high temperature

and high chloride concentration regimes, while avoiding galvanic prevention artifacts due to corrosion of the test frame.

- Use the accelerated test data to obtain by Arrhenius extrapolation preliminary bounding estimates of the likelihood of SCC developing for each alloy over a service life span of up to 100 years.
- With the information obtained from the accelerated tests, devise and implement a test procedure to evaluate the alloys at temperatures and chloride concentration regimes closer to those experienced in a marine environment as well as the effects of pore water on the initiation of SCC.
- Through these sets of experiments, determine which of the three stainless steel alloys tested is best suited for further evaluation for use as strand for prestressed concrete in a marine environment.

1.8 Approach

The set of experiments performed were separated into two parts or phases. In the first phase, the specimens of 316L, XM29, and 2205 were placed in a heating chamber, coated with $MgCl_2$ solution, and run from 135°C (275°F) down to 60°C or 140°F. Specimens were then evaluated at those temperatures for fixed time spans, removed and inspected. The time and temperature points of SCC initiation for each of the steels were found.

In the second phase, the temperature was lowered to 40°C (104°F) and 6 specimens (bent into a “U” shape) of each stainless steel were placed (for a total of 18 specimens) into a solution of 15 wt% Cl and a mixture of hydroxides and distilled water

that simulate pore water chemistry in concrete (also known as Synthetic Pore Solution [SPS]). This phase of the experiment was done in a sealed vessel, and showed through potential measurements the corrosion and/or absence of corrosion based on the potential symptoms associated with the passivation phenomenon as indicated earlier. While in the first phase there was a high concentration of chloride at the surface of the specimens, and is a worst-case scenario, the second phase parameters are more representative of an actual marine environment with the stainless steel acting as the strands in prestressed concrete.

Chapter 2: Methodology

2.1 Material Data

The three alloys tested were UNS # S31603, S24000, and S31803, commonly known as 316L, XM 29, and 2205, respectively.

The source for the material tested in these experiments was supplied by three manufacturing companies. The 316L 7-wire strand was supplied by National Strand Products Company in Houston, TX, the XM 29 7-wire strand was supplied by the Insteel Wire Products Company in Sanderson, FL, and the 2205 single wire was supplied by Carpenter Steel (Carpenter Technology Corporation) in Houston, TX. The diameters of each alloy wire were as follows: 4.36 mm (0.171 inches) for 316L, 4.47 mm (0.178 inches) for XM 29, and 4.56 mm (0.179 inches) for 2205.

Their yield strengths as reported by the manufacturers were: 1.24 GPa (180 ksi) for 316L, 1.59 GPa (230 ksi) for XM 29, and 1.59 GPa (230 ksi) for 2205. The following figures show the as-received condition of the 316L (Figure 4), XM29 (Figure 5), and 2205 (Figure 6).



Figure 4 Photo of Supplied 316L Material



Figure 5 Photo of Supplied XM 29 Material



Figure 6 Photo of Supplied 2205 Material

2.2 Specimen Preparations and Setup for Phase 1

For the first phase of the experiment the supplied material was cut into segments 114 mm (4.5 inches) in length. The strand segments of 316L and XM 29 were then unwound so one of the wires could be placed into a three-point bending frame. As shown in Figures 7a and 7b, an ~ 2cm long portion of the wire length on the tension side was coated with Magnesium Chloride (MgCl_2) crystals that absorbed moisture from the test cell's airspace creating a mixture (this mixture will be referred to as the "MgCl₂ slush") that is to remain saturated throughout the experiment.

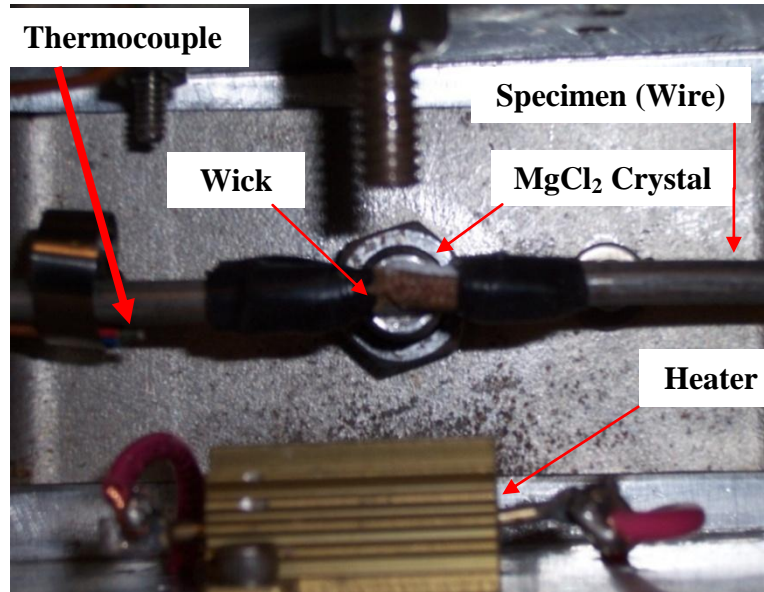


Figure 7a Bending Frame, Test Assembly, and Heater

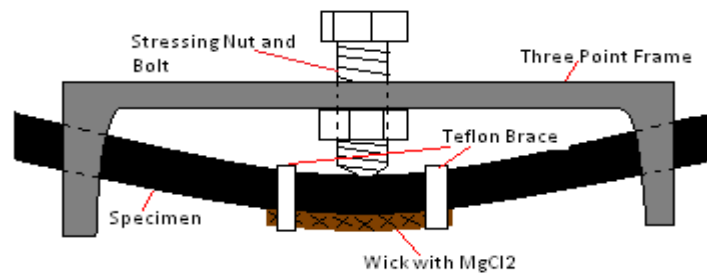


Figure 7b Diagram of Bending Frame

A wick was attached (using PRECISIONTAPE™ PTFE tape) to the wire to ensure the slush stayed against the wire throughout the experiment. The wire was then stressed by use of the three-point bending frame, and heated by a heating element underneath the frame.

The amount of stress applied by the bolt in the center of a three-point bending frame was calculated using equations relating the force applied by a bolt and nut combination (bolt/ nut) onto a specimen to the amount of revolutions of the bolt/ nut used.

First, W and F are calculated using the equations:

$$F = \tau_{\text{torque}} / (\mu * d) \quad (\text{Equation 3})$$

$$\text{and } W = t * F / d^2 \quad (\text{Equation 4})$$

where:

F is the amount of force the bolt/nut applies onto the specimen per area in psi,

t is the number of revolutions of the bolt/nut needed to put the force W on the specimen (in these experiments 3 revolutions were used),

W is the force on the specimen in lbf,

τ_{torque} is the tightening torque of the bolt/nut used in ft- lb,

μ is the coefficient of friction,

and d is the diameter of the bolt in inches.

The stress applied to the specimen is calculated using the equation:

$$\sigma_{\text{max}} = (P * a_{\text{frame}} * c) / I \quad (\text{Equation 5})$$

where:

P is 2*W, the force on specimen in lbf,

a_{frame} is the distance from center point of the frame to the outer points in inches,

c is the radius of specimen in inches,

and I is the moment of inertia in inches⁴[30].

The amount of stress applied to each specimen by the applied turns was calculated to be 1.15 GPa (167 ksi), 1.43 GPa (207 ksi) and 1.38 GPa (200 ksi) for the wires of alloy 316L, XM 29 and 2205 respectively. This corresponds to 93%, 90%, and 87% of the yield strength of each alloy respectively.

The bending frame was placed in a controlled enclosure that had pure water placed at the bottom which was heated to a temperature (T_1) corresponding to the water temperature needed for the Relative Humidity (RH) to be at 25% or greater in the enclosure. The temperature of the water in the enclosure was measured by a thermometer and controlled using a dimmer switch at the power supply and the heating controls on the enclosure. The enclosure was sealed to minimize the loss of water and ensure the air space above the water was at the appropriate RH. The RH is the actual vapor density of water in the air divided by the vapor density of water in the air at the saturation point for a given pressure and temperature. RH can also be expressed as the absolute pressure of the water in the air space divided by the absolute pressure of the water in the space heated for the experiment. The heating element under the frame then heated the wire to the temperature at which it was tested. The temperature of the wire (T_2) was measured by a thermocouple attached to the wire inside the test assembly containing the three-point bending frame and heating element. This thermocouple output also controlled the heating element through a process controller connected into the power loop of the heater. This setup caused the airspace around the test assembly to be at a different RH (RH_2) than the rest of the enclosure (RH_1). The testing enclosure is shown in Figure 8a and 8b.

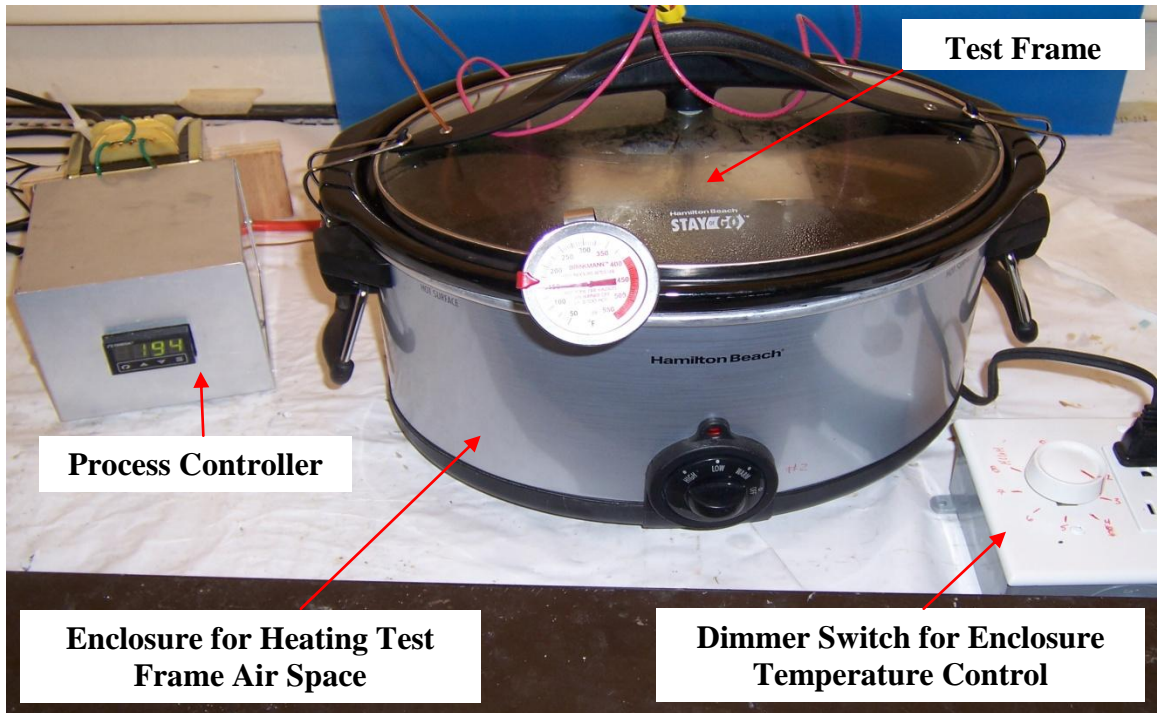


Figure 8a Phase 1 Test Enclosure

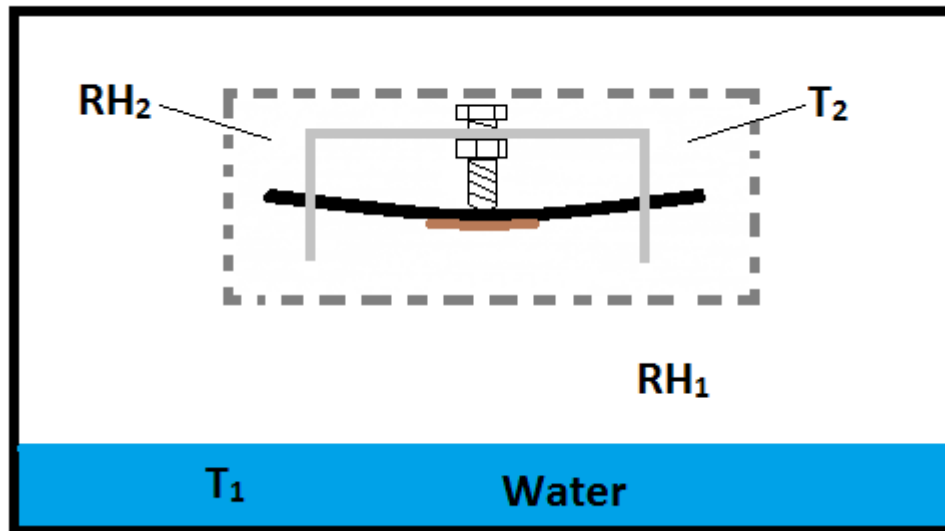


Figure 8b Diagram with Test Setup Process Parameters

The reason the RH must be maintained is that the wire is only affected by the MgCl_2 slush if the MgCl_2 slush is in a saturated solution, but will not be affected if the MgCl_2 is not. For SCC to occur the MgCl_2 slush must be acting as an electrolyte on the wire. Also, the MgCl_2 slush must not absorb too much water from the surrounding air or it will dilute to a concentration value too small to cause SCC. The state in which the MgCl_2 slush is in equilibrium with the water in the surrounding airspace is known as the Equilibrium Relative Humidity (RH_{eq}). The RH_{eq} has been calculated for various salts at the temperatures for which the experiment will be run as shown in Table 2.

Table 2 Equilibrium Relative Humidities for Salts at Various Temperatures

Temperature	NaCl (Sodium Chloride)	LiCl (Lithium Chloride)	MgCl_2 (Magnesium Chloride)
25°C (77°F)	75.29%	11.30%	32.78%
60°C (140°F)	74.50%	10.95%	29.26%
90°C (194°F)	~75.00%	10.23%	24.12%
135°C (275°F)	~75.00%	8.71%	14.27%

With the above information [31], and the steam tables for water [32] at the above mentioned temperatures, the RH that the specimen needs to be at was calculated for each temperature the specimens were tested at as shown in Table 3.

Table 3 Temperature versus Absolute Pressure of Water and the Relative Humidity for that Case

Temperature	Absolute Pressure of Water	Relative Humidity (RT Absolute Pressure/Absolute Pressure at the Temperature listed)
25°C (77°F)	0.029 atm (0.430 psi)	100%
60°C (140°F)	0.197 atm (2.890 psi)	14.88%
90°C (194°F)	0.686 atm (10.080 psi)	4.27%
135°C (275°F)	3.125 atm (45.920 psi)	0.94%

Note that from Table 3, at 60°C only LiCl would still be in solution for water at room temperature. Above 60°C even LiCl in pure water would be in a dry state.

Therefore, the water at the bottom of the testing enclosure needs to be heated so that the RH is equal to or greater than the RH_{eq} of the MgCl₂ at the temperature tested. Table 4 shows the temperature and pressure that the water at the bottom of the enclosure needs to be in order for the RH around the bending frame to be just above the RH_{eq} for MgCl₂.

Table 4 Temperature and Pressure of the Water at the Bottom of the Enclosure so that the Equilibrium Relative Humidity of MgCl is Equal to or Greater than the Relative Humidity at that Temperature and Pressure

Temperature of the air space near the specimen	RH _{eq} MgCl ₂ (Magnesium Chloride) at that Temperature	Absolute Pressure of Water needed to be at RH _{eq} or greater for MgCl ₂	Temperature of Water needed to be at RH _{eq} or greater for MgCl ₂
60°C (140°F)	29.26%	0.058 atm (0.846 psi)	36°C (97°F)
90°C (194°F)	24.12%	0.165 atm (2.431 psi)	56°C (133°F)
135°C (275°F)	14.27%	0.446 atm (6.553 psi)	79°C (174°F)

While running the experiment, it was noted that the RH needed to be at least 25% for the “slush” to form, and therefore, an increase in the water temperature of the enclosure of 4°C (25°F) above the values listed in Table 4 was required.

2.3 Specimen Preparation and Setup for Phase 2

For the second phase, the steels provided were cut down to 178 mm (7 inches) and unwound. For this phase, only the center or king wire of the 7-wire strand was used as it contains the least amount of curvature as compared to the outer wires. After cutting, the specimens were briefly (~< 1min) exposed to a 1 M nitric acid solution to clean off any low alloy steel particles that may have been embedded on the surface from the cutting process, degreased using ethanol, and rinsed with DI water.

Once cleaned, each specimen was placed in a bending jig (provided by Professor Gray Mullins) as shown in Figure 9, and bent into a “U” bend. Stainless steel plates with pre-drilled holes 32 mm (1.27 inches) apart were then placed onto the specimens to hold to them in the “U” bend.



Figure 9 Bending Jig with 316L Specimen

Measurements of the amount of springback each specimen had after bending occurred. These measurements provide another method by which to determine if SCC occurred in the specimens. If the specimen after testing did not springback as much as before the test, then this reduction in springback would be a sign that the material has become brittle and SCC occurred. Figures 10a, b, c, d, e, and f show the measurement of relaxation (springback) of each specimen as well as the bent condition held in place by the plates. The location the plate would rest on was marked on the outer diameter side of each specimen. The difference between the outer diameter distance (measured using the marks mentioned previously) relaxed and the outer diameter distance bent gives the amount of springback. Table 5 shows those values.

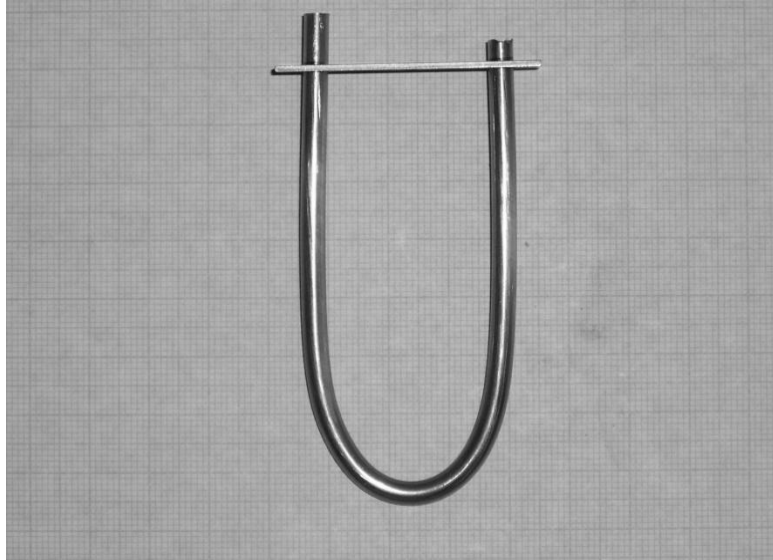


Figure 10a Bent 316L Specimen (1sq =1 mm)

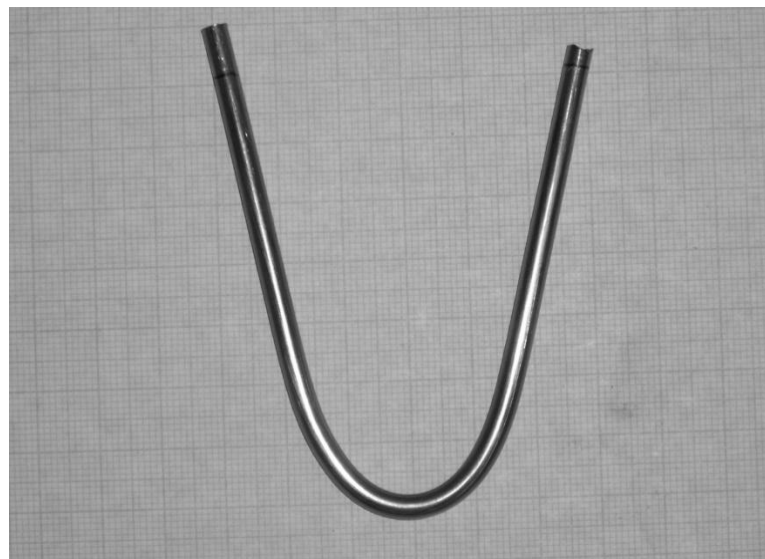


Figure 10b Relaxed 316L Specimen (1sq =1 mm)

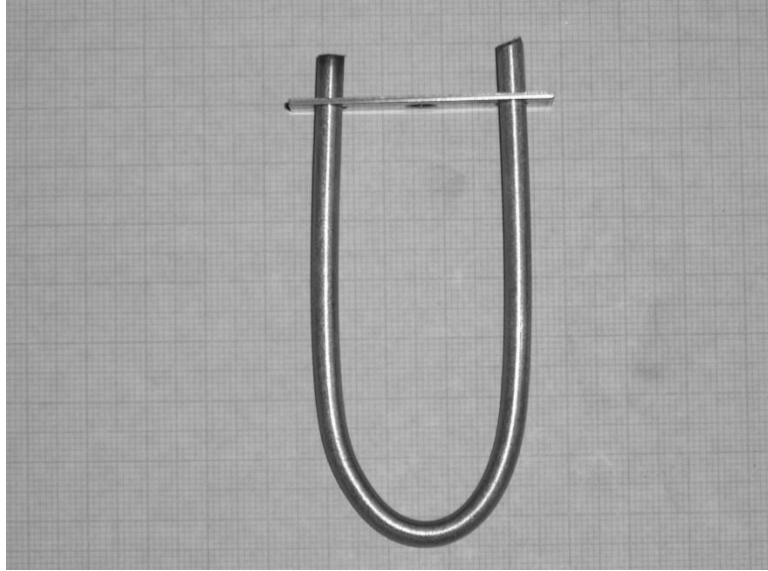


Figure 10c Bent XM 29 Specimen (1sq =1 mm)

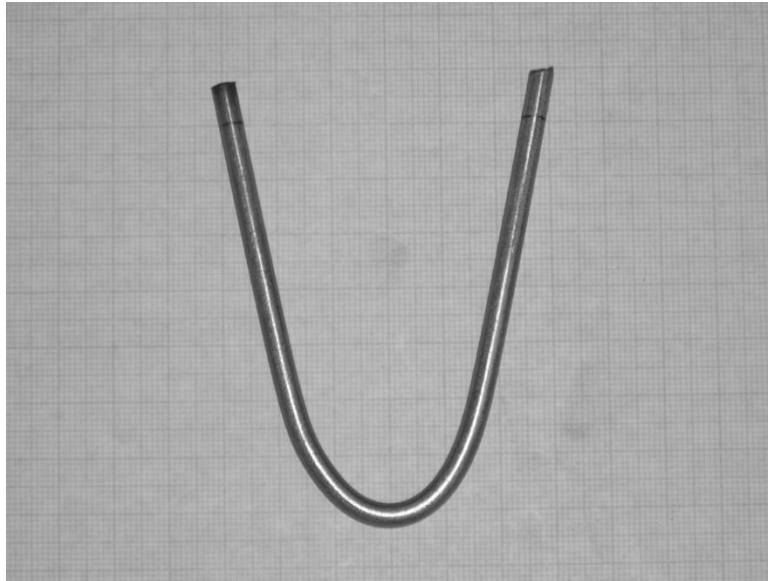


Figure 10d Relaxed XM 29 Specimen (1sq =1 mm)

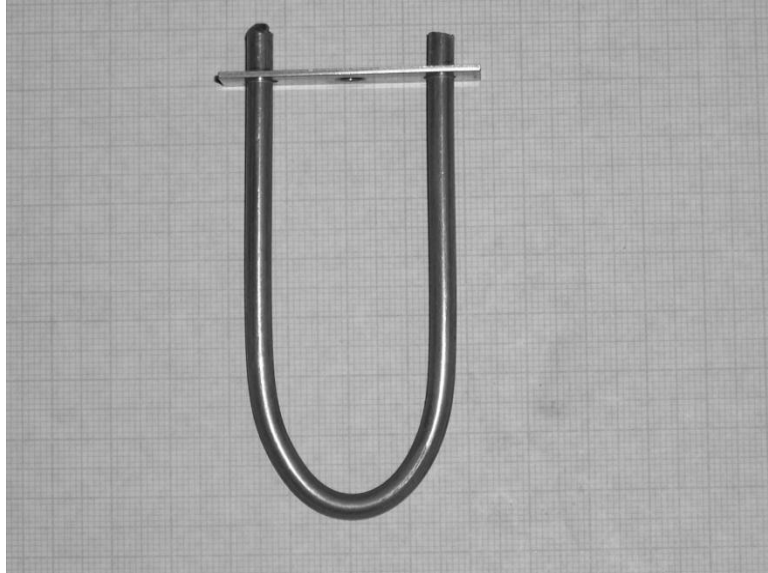


Figure 10e Bent 2205 Specimen (1sq =1 mm)

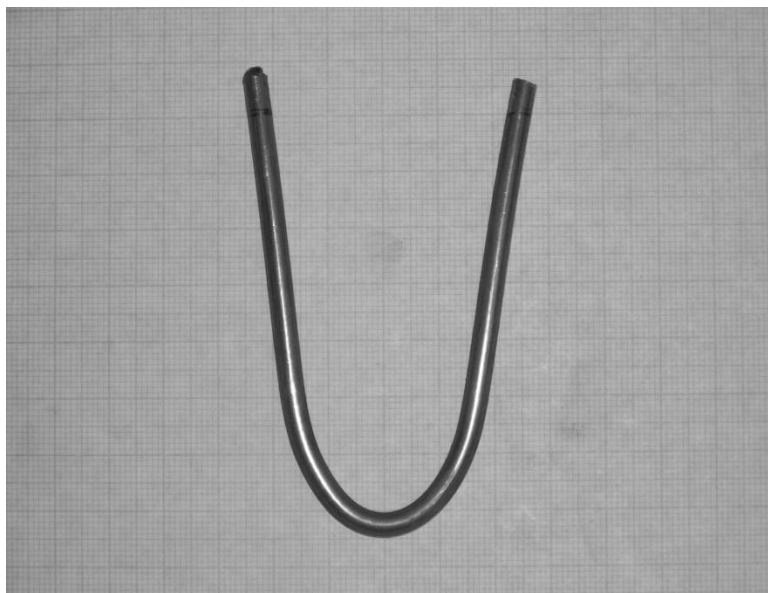


Figure 10f Relaxed 2205 Specimen (1sq =1 mm)

Table 5 Springback Amount for Each Alloy (in mm/ inches)

Specimen Alloy	Relaxed Distance	Bent Distance	Difference
316L	60.1/ 2.37	34.8/ 1.37	25.2/ 0.99
XM 29	59.2/ 2.33	34.8/ 1.37	24.4/ 0.96
2205	51.3/ 2.02	34.8/ 1.37	16.3/ 0.64

2.4 Insulating Enclosure and Tank Setup

For phase 2, specimens of each type of stainless steel were placed in a large container (12 inches inside diameter and 15 ½ inches tall) in a solution of 15wt% Cl containing NaOH, KOH, Ca(OH)₂, and pure water to simulate concrete pore water . The solution was heated to 40°C (104°F). The preparation protocol is as follows.

The volume of solution needed is first calculated by calculating the volume of the vessel:

$$V=h*\pi*(D/2)^2 \quad \text{(Equation 6)}$$

where:

h is the depth of the solution desired (2.5 inches),

and D is the diameter of the vessel.

The total volume of final solution needed to cover the specimens while leaving 1 inch from the surface of the solutions to the mounting plate is 4.633 liters.

The following calculations provide the amount of each component needed to make about 4.633 liters of final solution.

- For NaOH:

Assume that NaOH is the only solute when finding the density of the solution of NaOH and water. This can be assumed due to the much larger percentage of water when compared to the percentage of NaOH and KOH to be added. Concentration of NaOH in base solution is 8.33 g/L (per Table 6). Data for finding the density of NaOH in water comes from Table 68 [33]:

C (g/L)	Density (Kg/L)
5	1.0039
10.1	1.0095

Interpolating, the density of NaOH in water solution is $((8.33-5)/(10.1-5))*(1.0095-1.0039)+1.0039=1.0076$ kg/L.

- For KOH:

Assume that KOH is the only solute when finding the density of the solution of KOH and water. Concentration of NaOH in base solution is 23.3 g/L (per Table 6). Data for the finding density of NaOH in water comes from Table 45 [33]:

C (g/L)	Density (Kg/L)
20.3	1.0155
25.5	1.0198

Interpolating, the density of KOH in water solution is $((23.3-20.3)/(25.5-20.3))*(1.0198-1.0155)+1.0155=1.0180$ kg/L.

The density of water was obtained from page F-11 Figure 2 [33] and is 0.9982 kg/L. Since the additions to the water to make the base solution are small compared to the amount of water, it is assumed that the effect of the total additions to make the base solution is equal to the sum of the effects of the individual additions. Base solution density is therefore equal to $0.9982+(1.0076-0.9982)+(1.0180-0.9982)=1.027$ kg/L. The mass of the base solution is therefore 1 liter times the density of 1.027 kg/L which equals 1.027 kilograms.

The mass of Cl needed to make 15wt% Cl solution starting with 1 L of base solution is x_{Cl} such that $(x_{Cl}/(x_{Cl}+x_{Na}+1.027)) = 0.15$, where $x_{Na} = x_{Cl}*(AW_{Na}/AW_{Cl})$ and atomic weights (AW) of Sodium is 22.99, Chlorine is 35.453 and Sodium Chloride is 58.443, which leads to $x_{Cl} = 0.205$ kg. Using the $x_{NaCl} = x_{Na} + x_{Cl} = x_{Cl} (AW_{Na} /AW_{Cl})+x_{Cl} = x_{Cl} ((AW_{Na} /AW_{Cl})+1)$, the mass of NaCl needed for 15wt% Cl is $x_{NaCl} = 0.337$ kilograms.

To get 15wt% Cl in the base solution, 0.337 Kg of NaCl is added to 1 L of base solution with a mass of 1.027 kg, to get a total of 1.364 Kg of solution.

It is conservatively assumed that when obtaining the concentration of NaCl in the final solution, all additions to the solution are NaCl solute (as it has the highest density of the three additions [NaOH, KOH, NaCl] so the mass of the NaCl solute is $337+23.3+8.33=368.99$ g).

To obtain the concentration of NaCl in the final solution, take the total mass of the solute and divided it by the total mass of the final solution $368.99 \text{ g} / 1.364 \text{ g} = 27\%$.

For the final solution 15wt% Cl (which is the base solution plus the addition of 337 g of NaCl). Data for finding the density of the final solution comes from Table 64 [33]:

% by Weight Density (Kg/L)

25% 1.1887

26% 1.1972

Interpolating, for the final solution 15wt% Cl: 26% by weight -25% by weight +26% by weight =27% by weight which is the same as the concentration calculated above, and therefore $1.1972 \text{ Kg/L} - 1.1887 \text{ Kg/L} + 1.1972 \text{ Kg/L} = 1.206 \text{ Kg/L}$.

The volume of the final solution is the total mass of the final solution (1.364 kg) divided by the density (1.206 kg/L) gives a volume of 1.13 liters.

Table 6 Desired Base Solution Composition for 15 wt% Cl and SPS Solution (Table 3 [34])

TABLE 3
Chemical Composition (g/L) and pH Values of Model Solutions

	Ca(OH) ₂ ^(A)	NaOH	KOH ^(B)	Na ₂ CO ₃	NaHCO ₃	pH ^(C)	pH ^(D)
SCS	2.0	—	—	—	—	12.6	12.0
SPS	2.0	8.33	23.3	—	—	13.6	13.0
CPA	—	—	—	4.21	2.66	9.7	8.6

^(A) Most of the Ca(OH)₂ was not dissolved.

^(B) Reagent-grade KOH had a purity of only 85.3%.

^(C) Before addition of Cl⁻.

^(D) With 15% Cl⁻.

The steps to prepare 1 liter of base solution are:

- Add target 8.33 grams of NaOH and 23.3 grams of KOH to a 1 liter volumetric flask. Weigh and record actual amounts of each solid added per precise zeroed-out balance reading.
- Add distilled water to fill up to the liter reference line. Shake gently.
- Weigh and record actual amount of Ca(OH)₂ for a target value of 2 grams and set aside.

The steps to prepare 1.13 liters of 15wt% Cl solution starting from 1 liter of the base solution are:

- Transfer 1 liter of base solution to test vessel.
- Add target 337 grams of NaCl to test vessel. Weigh and record actual amount of solid added per precise zeroed-out balance reading.
- Add the pre-weighed 2 grams of Ca (OH)₂ to the vessel solution. Stir mixture fully.

Repeat the above procedure 3 more times to make a total of 4.633 liters of the 15wt% Cl⁻ solution. Also, since the solution is to be heated, the possibility of a drop in pH (which should stay above 12.5 pH to be similar to pore water in concrete) was a concern. The SPS solution was therefore tested for its pH periodically, using a pH meter. Normally, most pH meters only accurately read up to about pH 10, so a calibration and measurement procedure was needed. The procedure involved taking the millivolt reading on the pH meter for known buffer solutions of pH 4, 7, 10, 13 and 14. Then the measurement of the solution occurred by removing a sample of the solution, allowing it to cool naturally in a sealed container, and then measuring the millivolts with the pH meter. Calculating the slope of the millivolts versus pH curve, and finding where the measurement for the solution (in millivolts) lies in respect to the pH, a pH for the solution can be estimated. During all of the measurements, including the pH buffer ones, the temperature was taken, and pH values were adjusted based on the temperature measured. All pH values measured throughout the 90 days of the phase 2 experiment were above 12.5 and within the range of 12.5 and 13.5.

The specimens were suspended from a positioning frame by stainless steel rods in a enclosure fitted with a heating patch near the bottom to heat the solution to the needed temperature.

A process controller, similar to the one used for the first test, was setup to maintain the temperature of the solution within the container. Two calibrated thermocouples were placed in two different points of the solution to ensure uniform temperature measurements of the solution. The top of the enclosure was sealed, and all wires for potential and temperature measurements went through air-tight fittings in the

wall of the enclosure. The reason Phase 2 was done in a sealed up enclosure was to mitigate evaporation of the SPS & 15 wt% Cl solution from the tank as well as blocking atmospheric CO₂ from coming into the container and causing carbonation of the SPS & 15 wt% Cl solution. The entire setup was insulated to assist in the maintaining of the temperature of the test cell. An agitator was used to ensure the mixture is thoroughly mixed as well as to ensure a uniformity in the solution temperature by moving the liquid past the heating pad. The uniformity of the temperature of the solution is an important factor in this phase, as the test results would not be valid if the temperature was different at different locations in the solution. This is due to the different location of specimens throughout the volume of the enclosure.

Figures 11a, 11b, 11c and 12 show the setup of the second phase positioning frame and the wiring of the process controller and relays.



Figure 11a Phase 2 Test Enclosure

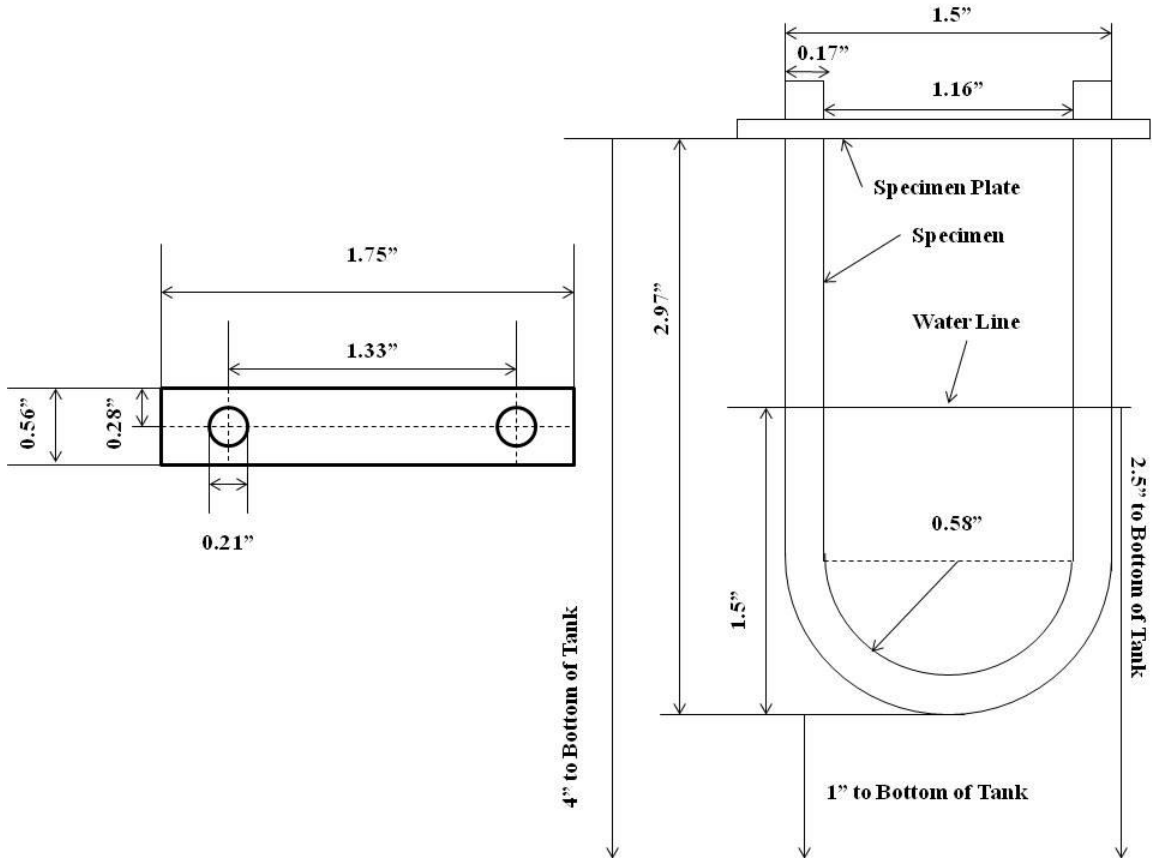


Figure 11b U-Bend Specimen Dimensions

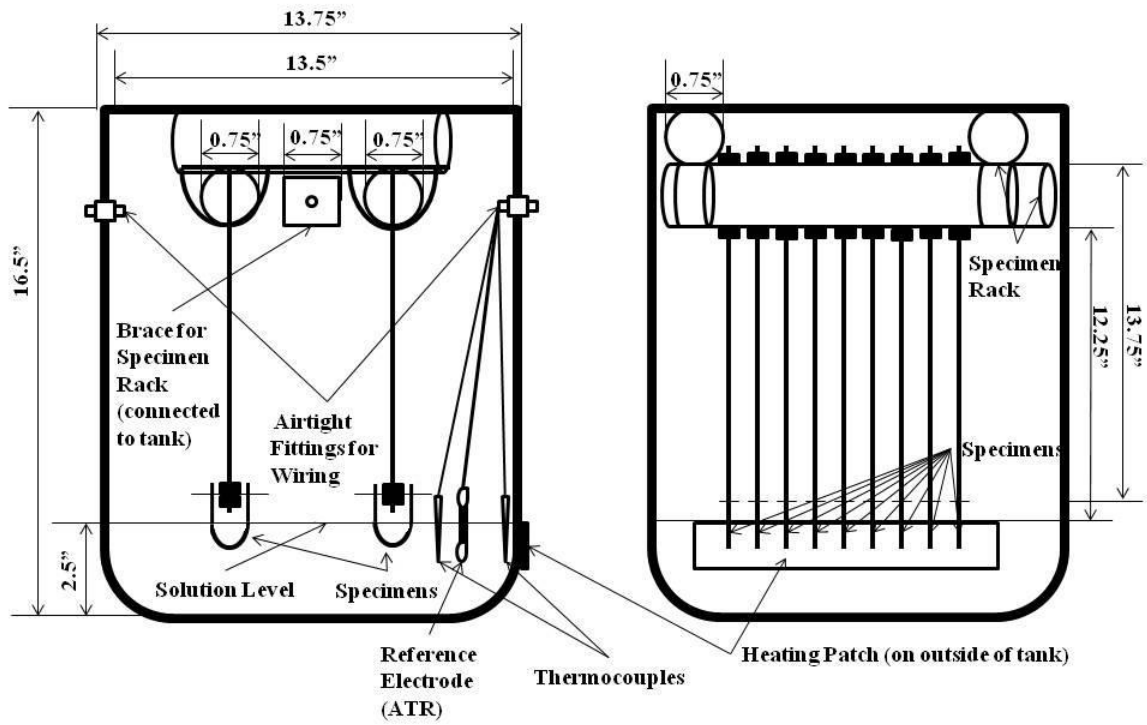


Figure 11c Diagram of Overall Insulated Tank Setup

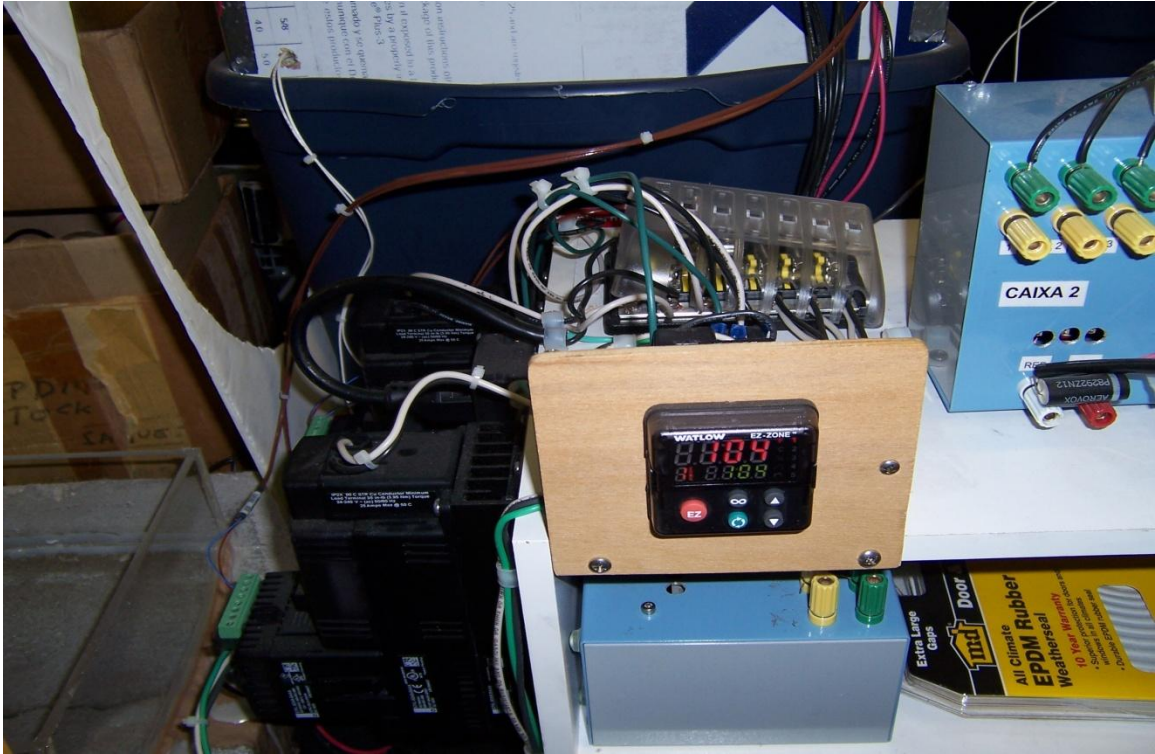


Figure 12 Process Controller and Wiring Setup for Second Test

Chapter 3: Results

3.1 Phase 1 Results

After each run, the specimen tested was inspected for cracks. First, the specimen was inspected while in the bending frame still under stress. If no cracks were observed, the specimen was then bent farther into a full 90° U-Bend. If cracks were observed at either point, that time or temperature was noted as SCC occurring for that alloy. If no cracks were detected, it was noted that no SCC occurred in that alloy for that exposure time and temperature.

Table 7 lists the results of all three cases for the first phase using MgCl₂ and pure water to test for SCC in a heated air space. If SCC occurred, the result is an X, if not, an O. When the tests showed a specimen having SCC at a short time span, it was assumed that SCC would happen at a longer time span for that alloy. Runs not done on an alloy are noted on Table 7 by a dash.

In the following it will be assumed that the SCC process is activation controlled with a rate r following an Arrhenius relationship:

$$r_{\text{corrosion}} = c_0 \exp(-Q/RT) \quad (\text{Equation 7})$$

where:

c_0 is a constant,

Q is the activation energy for the process,

R is the gas constant,

and T is the absolute temperature in °K.

If the rate of the process is assumed to be simply inversely proportional to the time transurred until the observation of a stress corrosion crack, (t_{SCC}) then the times for observing SCC when an alloy is tested at 2 different temperatures, t_{SCC1} and t_{SCC2} are given by:

$$t_{SCC2}/t_{SCC1} = \exp(-Q/[R*(1/T_1-1/T_2)]) \quad (\text{Equation 8})$$

Solving for Q, the equation is:

$$Q = \ln(t_{SCC2}/t_{SCC1}) * [R(1/T_1-1/T_2)] \quad (\text{Equation 9})$$

The activation energy calculated using the Arrhenius Relationship and the data obtained for 316L is $Q=71.5$ kJ/mol and for XM 29 is $Q=81.3$ kJ/mol. Because of lack of data at this time for 2205, the activation energy was not calculated for it. The activation energy calculated for these reactions were well within the range of activation energies expected and found in the literature (between 70 kJ/mol and 100 kJ/mol) [28].

This approach was used to estimate values of Q for each of the alloys tested. Equation 9 corresponds to a straight line in a $\log t = f(1/T)$ graph, where the slope of the line is directly proportional to the value of Q. Figure 28 uses that format to display the results of all the Phase 1 SCC experiments. Using the different times and temperature information for 316L, XM29, and 2205 cracked, the slope of the log time versus inverse temperature can be calculated, and is shown on Figure 28 as a red line for 316L, as a green line for XM29, and a dotted blue line for 2205. For 2205, there is not enough data to do a full extrapolation, so the data available was used plus the averaging of XM 29 and 316L information to estimate a slope and intercept.

The value of t_{SCC} for a given alloy at a given temperature was estimated by finding the logarithmic average of the lowest time for cracking observed for a given alloy at a certain temperature, and the shortest time for which cracking was not observed. Once these t_{SCC} values were found for at least two different test temperatures, the slope that yields the value of Q could then be calculated.

With knowledge of the value of Q , the proportionality constant can be calculated. Lines representing Equation 7 were drawn accordingly in the diagram of Figure 28. The lines were extrapolated towards lower temperatures. A temperature of 40°C (104°F) was chosen as being representative of worst-case field conditions expected in a sub-tropical service environment such as that of Florida. Therefore, the interception of the sloping line for each alloy with the vertical line corresponding to 40°C (104°F) yielded an appropriate estimate of the time for development of SCC for each alloy in the test medium used for the Phase 1 experiment. Those times are listed next to the dashed lines corresponding to the alloys and are shown on Figure 28.

Figure 28 shows that at 40°C (104°F), XM 29 would have SCC initiated after 82 years. 2205 and 316L show much lower times at that same temperature, 2.3 and 0.06 years respectively. The graph also shows that XM 29 performance in the Phase 1 tests was significantly better than that of both 316L and 2205 with t_{SCC} values at least two orders of magnitude higher than both 316L and 2205. It is also noted that there was little or no sign of corrosion on the bending frame used for all alloys, indicating that the artifact of galvanic prevention was prevented in Phase 1. Therefore, the effect of galvanic prevention due to the coupling of the specimen with the bending frame showed to be significant to the SCC susceptibility comparison between 316L and XM 29. With

galvanic prevention, 316L can endure 90 days at 106°C without signs of corrosion, but without galvanic prevention cannot last more than 4 days at 90°C without corroding.

The results are encouraging for XM 29 as the t_{SCC} exceeds the 75 year service life criteria adopted by the Florida Department of Transportation. The results for alloys 316L and 2205 show that those alloys would not even reach 5% of the service life criterion.

However, it should be noted that these are conservative estimates as the test used in Phase 1 does not include mitigating substances such as those present in concrete pore water that elevate the pH to highly alkaline values and may delay corrosion initiation. It should also be noted that as the lines are extrapolations and therefore the times listed for 40°C are estimates and are the average of a range of data (confidence range) inherent in the extrapolation done for that data.

**Table 7 Results of Phase 1 Experiment Using MgCl₂ and Pure Water
X: Cracking; O: No Crack**

Specimen Temperature °C (°F)	Run Time hours	316L Specimen # /Result	XM29 Specimen # /Results	2205 Specimen # /Results
135 (275)	48	A1/ X	B1/ X	-
135 (275)	24	-	B3/ X	C4/ X
135 (275)	4	A2/ X	B2/ O	C5/ X
135 (275)	1	A3/ X	B4/O	C6/ X
90 (194)	1344	-	B13/O*	-
90 (194)	672	-	B12/ O	-
90 (194)	336	-	B11/ O	-
90 (194)	168	-	B10/ O	-
90 (194)	96	A4/ X	B6/O	C9/ X
90 (194)	48	A5/ X	B5/ O	C8/ O
90 (194)	24	A6/ X	B7/ O	C7/ O
90 (194)	4	A7/ X	-	-
90 (194)	1	A8/ O	-	-
60 (140)	168	A9 / X	B8/ O	C3/ O
60 (140)	96	A12 / X	-	C1/ O
60 (140)	24	A10 /O and A11 /O	-	C2/ O

*Note: Specimen B13 had no SCC, but did have pitting corrosion, which may have cathodically prevented SCC from occurring. It is therefore conservatively assumed that SCC occurred after 8 weeks only for the purpose of activation calculation and the slope of the green line in Figure 28.

Table 7 indicates that 316L at 135°C (275°F) began SCC within an hour, while XM29 requires at least a day under the same conditions. It also indicates that 316L at 90°C (194°F) began SCC within a day, while XM29 did not crack after 4 days or more under the same conditions. Lastly, Table 7 indicates that 316L at 60°C (140°F) began

SCC after 4 days, while XM 29 did not crack after a week or more under the same conditions. Alloy 2205 performed better than 316L at 60°C (140°F) and 90°C (194°F), but the same at 135°C (275°F). Therefore, 2205 performs better than 316L, but not as well as XM29 in Phase 1.

Figures 13 through 27 show the results of Phase 1 for the specimens labeled per Table 7. Only specimens with cracks showing SCC occurred are pictured below. All pictures were taken at 25X magnification.

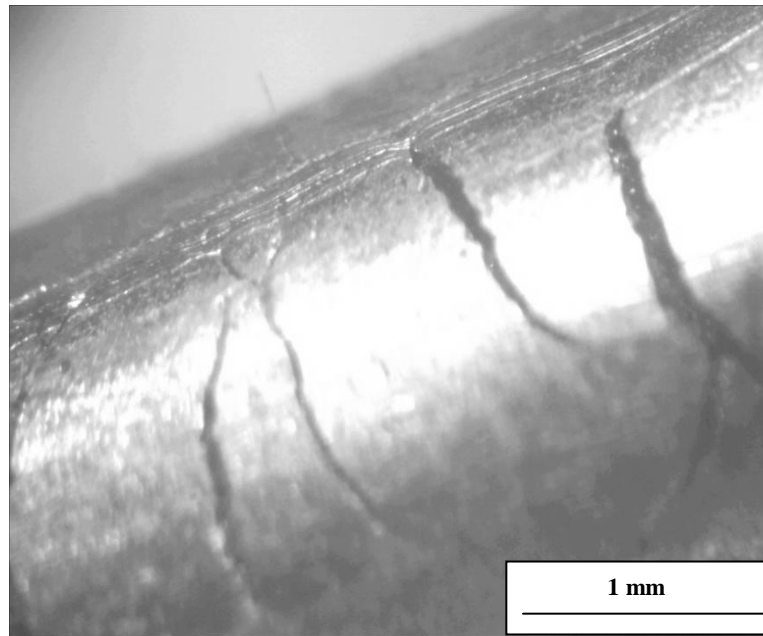


Figure 13 Specimen A1 316L @135°C (275°F) Cracked after 48 Hours

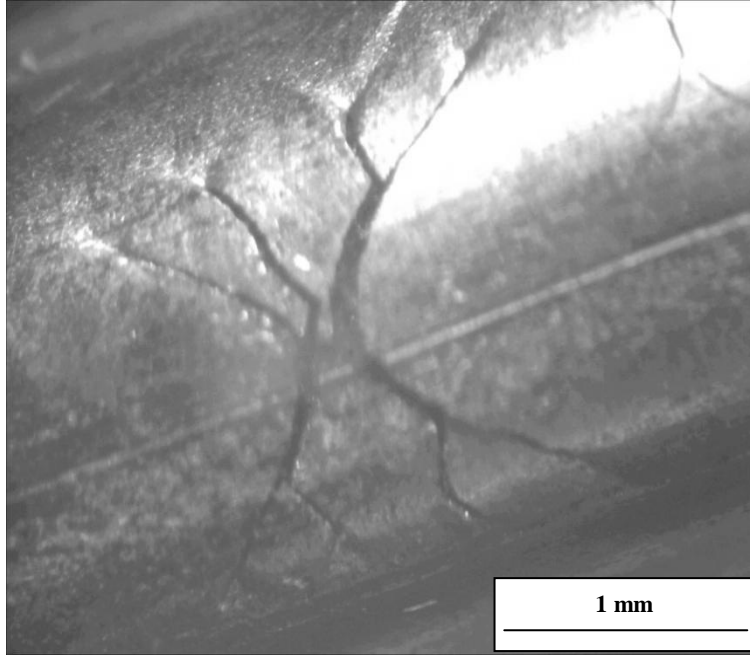


Figure 14 Specimen A2 316L @ 135°C (275°F) Cracked after 4 Hours

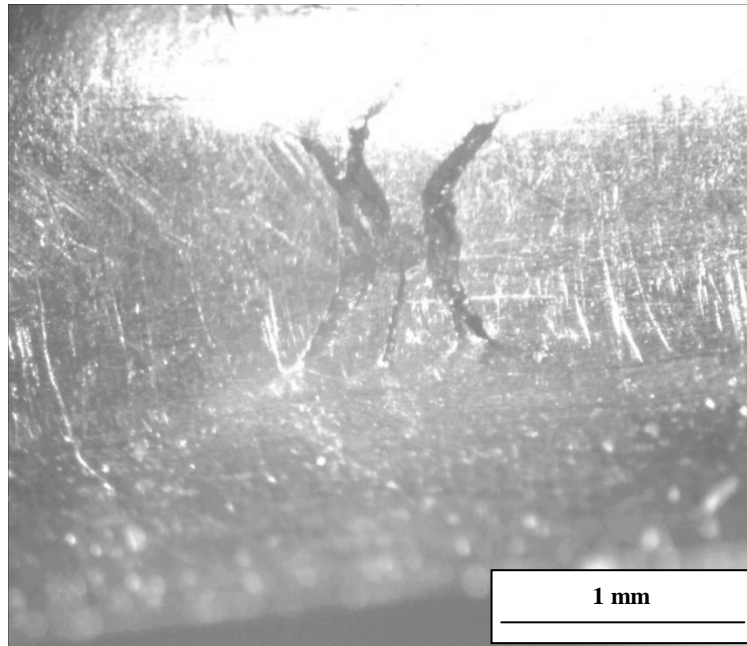


Figure 15 Specimen A3 316L @ 135°C (275°F) Cracked after 1 Hour

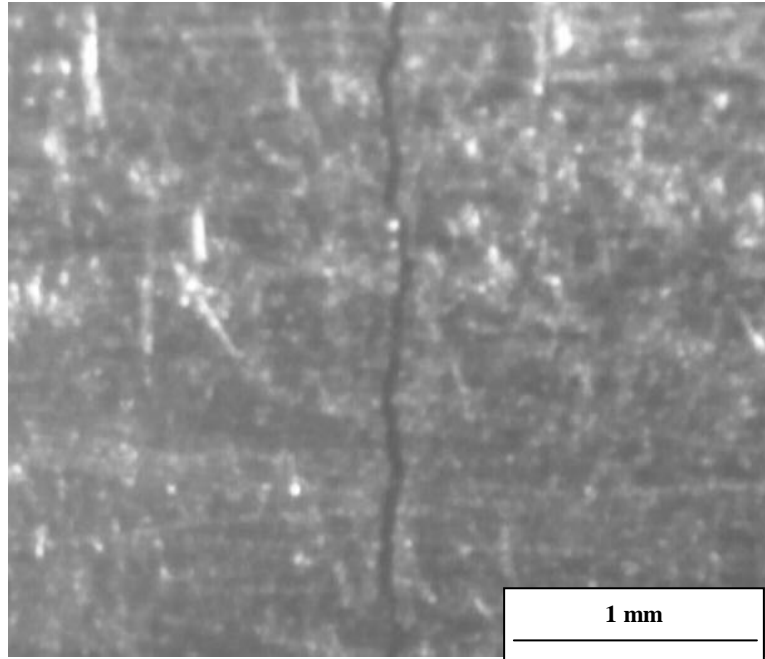


Figure 16 Specimen A4 316L@ 90°C (194°F) Cracked after 96 Hours

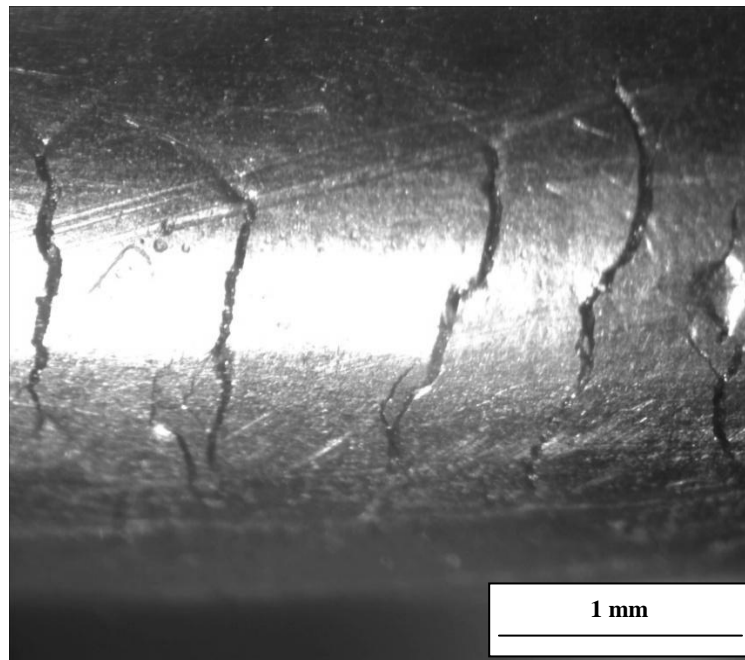


Figure 17 Specimen A5 316L @90°C (194°F) Cracked after 48 Hours

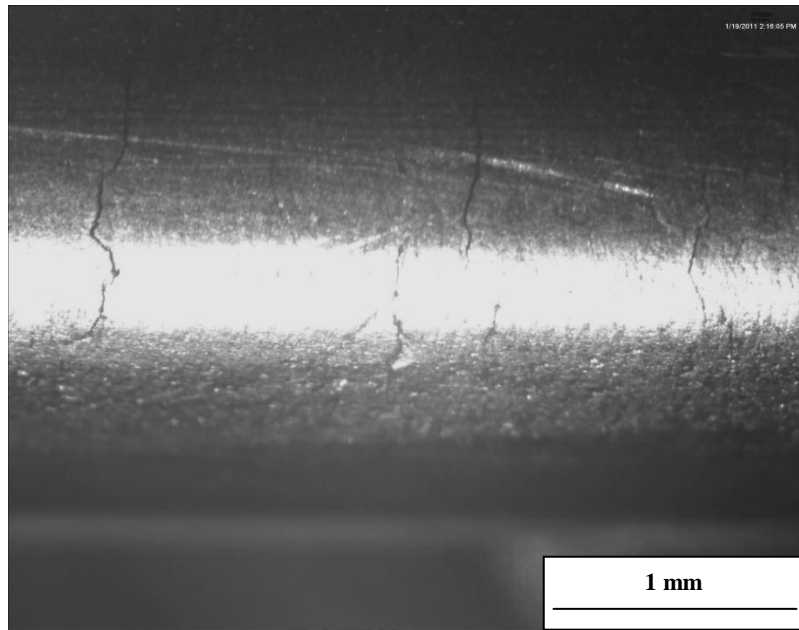


Figure 18 Specimen A6 316L @90°C (194°F) Cracked after 24 Hours

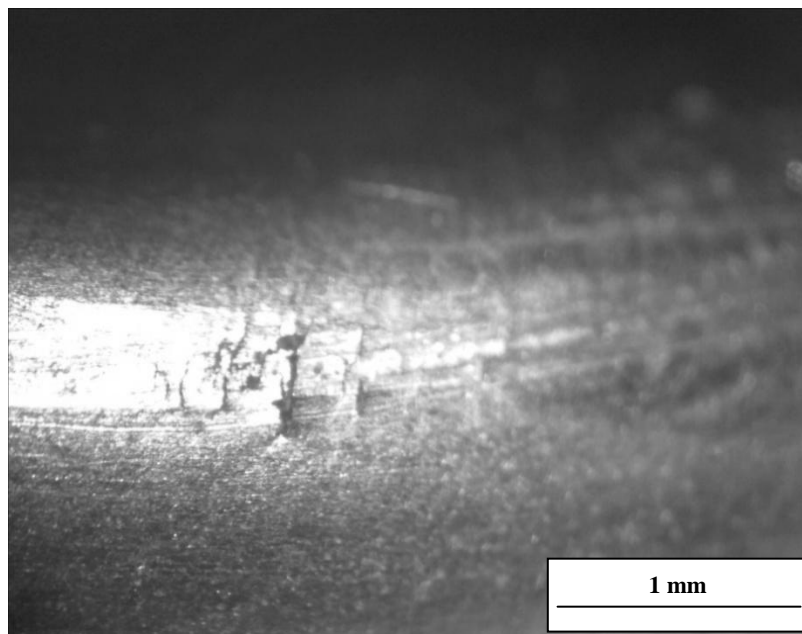


Figure 19 Specimen A7 316L @90°C (194°F) Cracked after 4 Hours

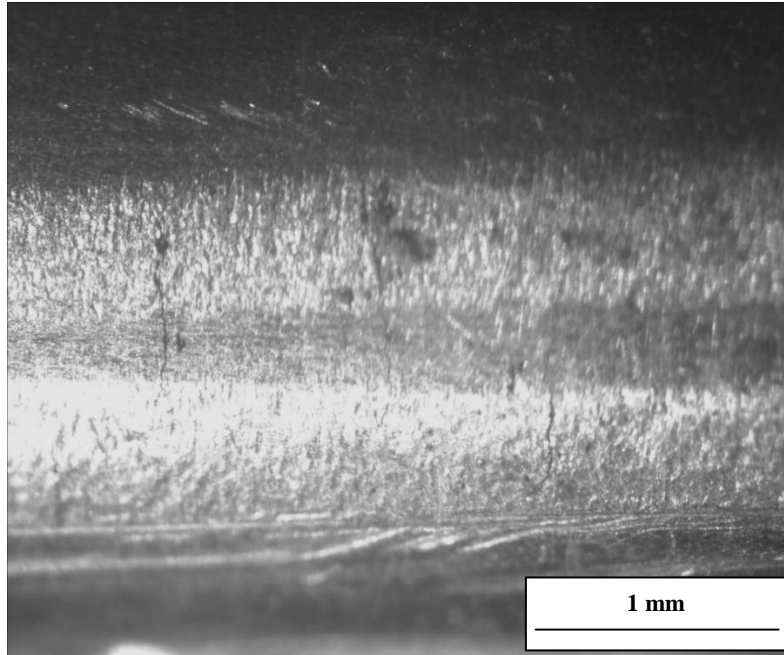


Figure 20 Specimen A9 316L @60°C (140°F) Cracked after 168 Hours

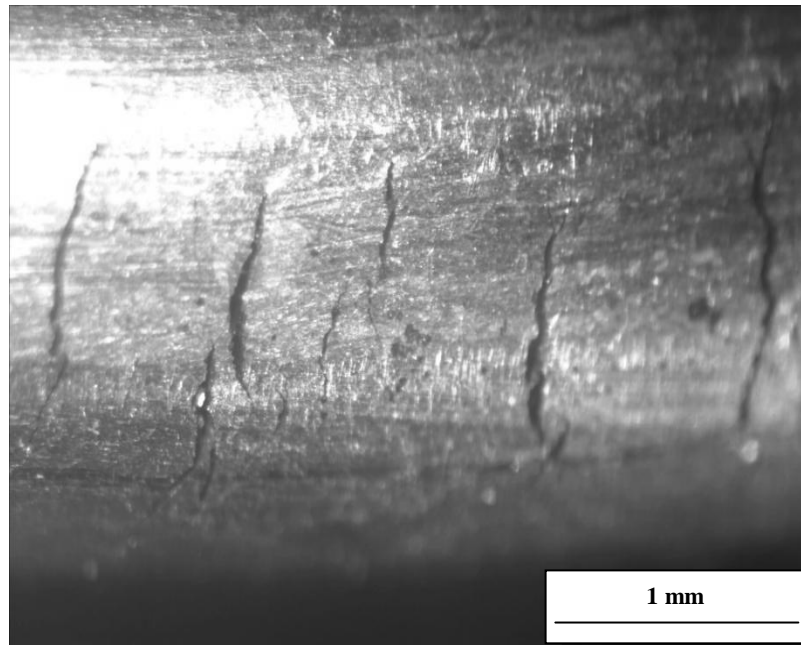


Figure 21 Specimen A12 316L @60°C (140°F) Cracked after 96 Hours

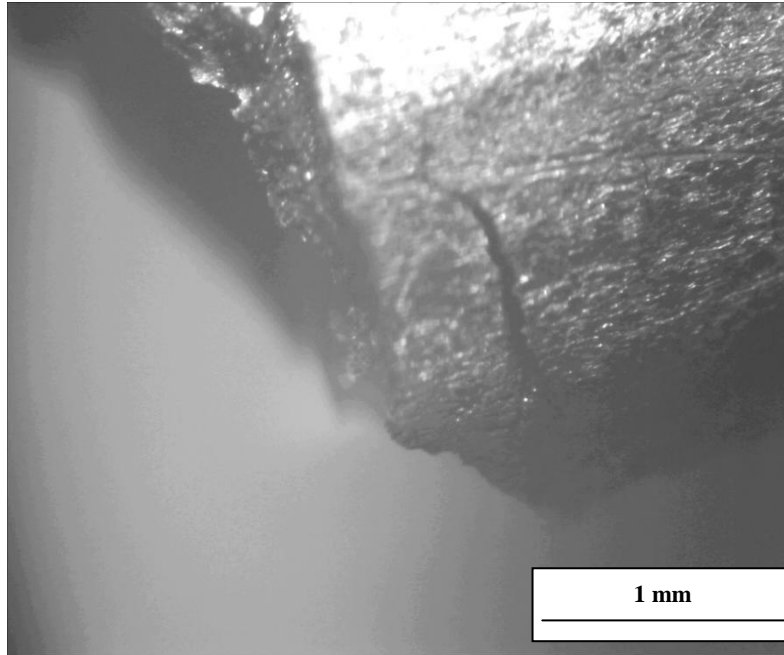


Figure 22 Specimen B1 XM 29 @ 135°C (275°F) Cracked after 48 Hours

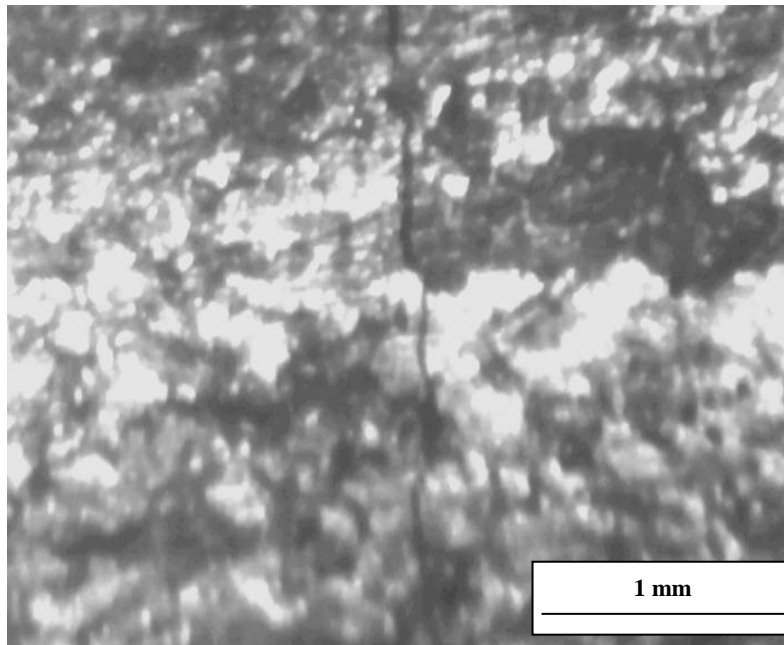


Figure 23 Specimen B3 XM29 @135°C (275°F) Cracked after 24 Hours

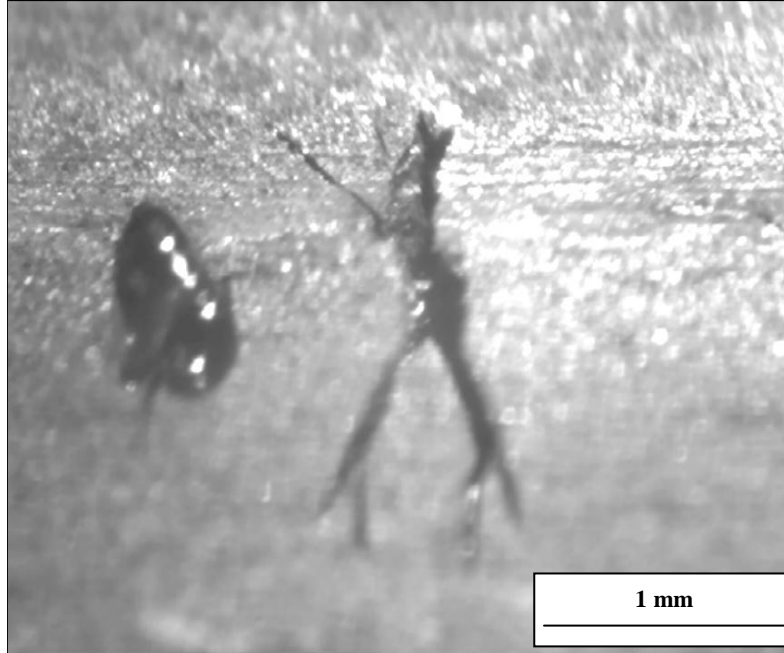


Figure 24 Specimen C4 2205 @135°C (275°F) Cracked after 24 Hours

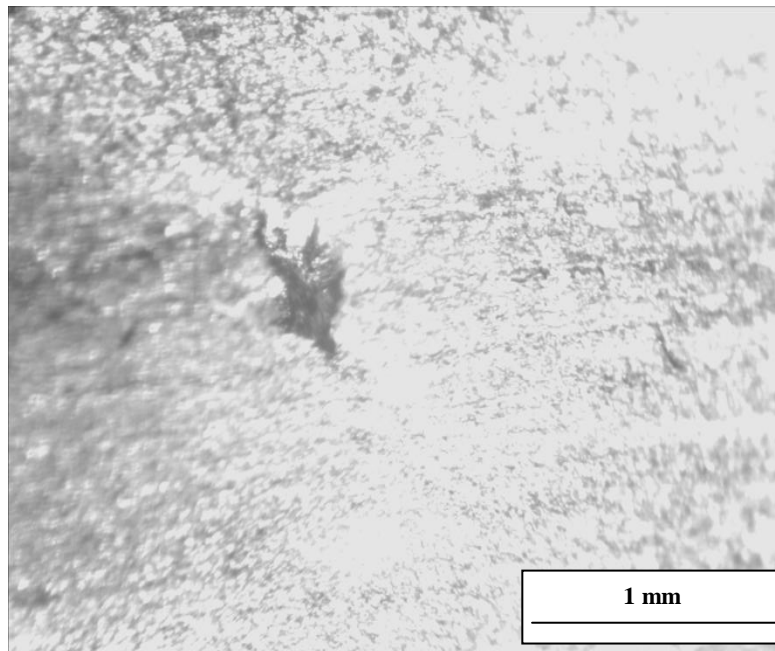


Figure 25 Specimen C5 2205 @135°C (275°F) Cracked after 4 Hours

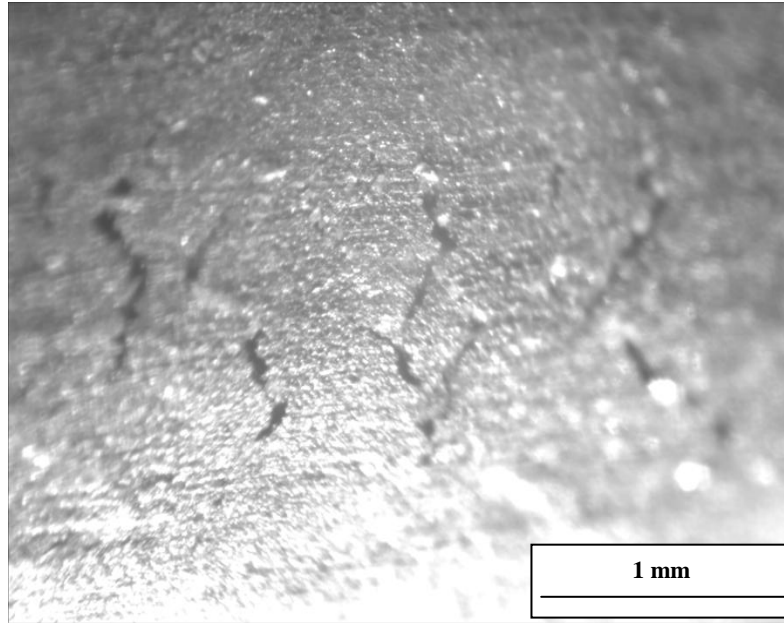


Figure 26 Specimen C6 2205 @135°C (275°F) Cracked after 1 Hour

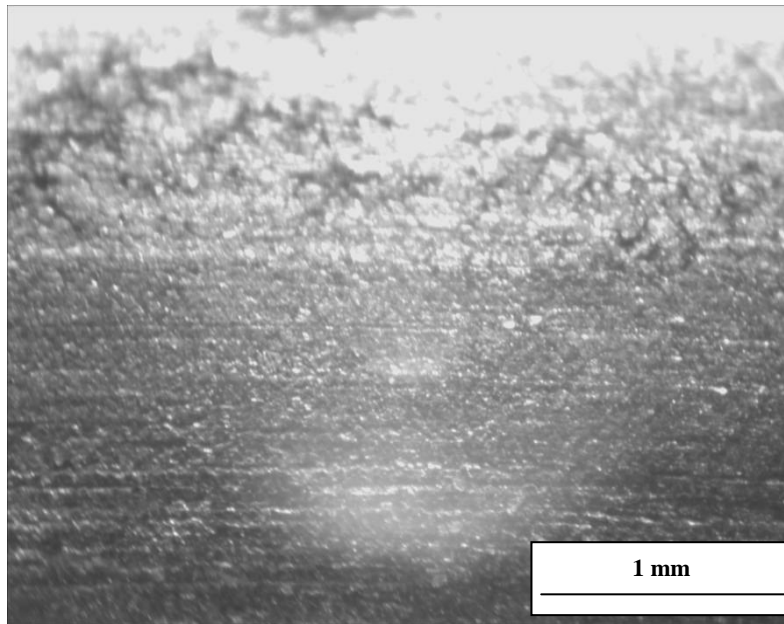


Figure 27 Specimen C9 2205 @90°C (194°F) Cracked after 96 Hours

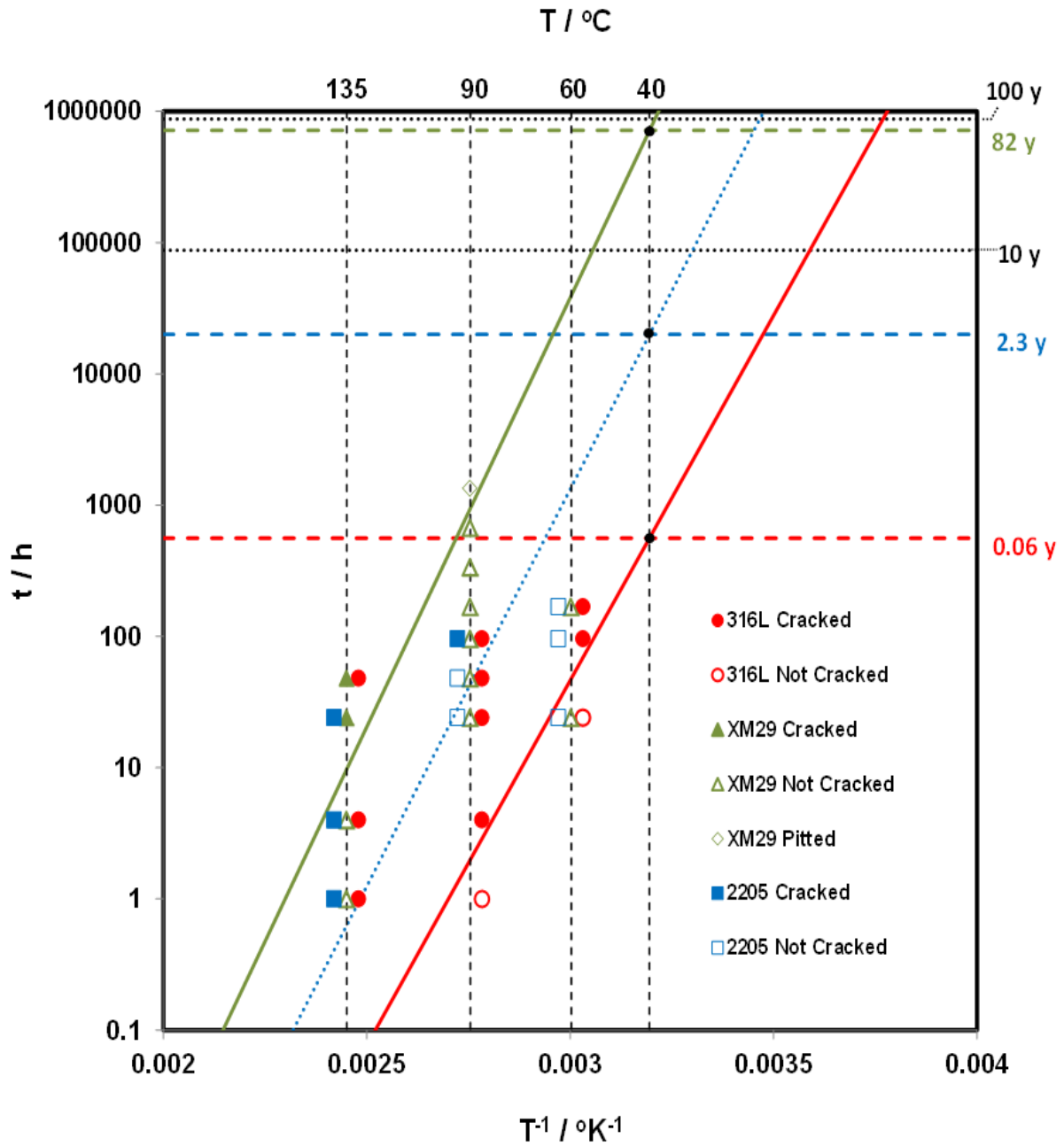


Figure 28 Graph of Exposure Time (Log Scale) Indicating Test Outcome, as Function of Inverse Absolute Temperature. Some Data Offset Left and Right for Display Clarity. Sloping Lines Indicate Arrhenius Abstraction of the Results. Nominal Time to SCC at 40°C is Obtained for each Material by Extrapolation. The 10 Year and 100 Year Markers are Shown for Contrast

3.2 Phase 2 Results

In Phase 2, the specimens were connected to wiring which allowed the measurement of the open circuit potential using a multimeter and an Activated Titanium Reference (ATR) electrode. These measurements were done at least once a day for all 18 specimens, and graphed. These graphs serve to detect any potential change in the specimens that would indicate the initiation of SCC. Open circuit potential measurements performed during the 2160 hour Phase 2 runs are presented in Figures 29, 30, and 31. The specimens were also visually inspected numerous times throughout the 2160 hours. Neither periodic visual examination of the surface of the specimens during the 2160 hour test period, nor detailed microscopic examination with a stereo-zoom microscope after the specimens were removed from the test enclosure revealed any recognizable signs of SCC in any of the specimens.

Of the 18 specimens tested, only three of the specimens showed a somewhat different trend in potential (as compared to the other specimens of the same alloy). Those specimens are #1 (316L), #9 (XM29), and #15 (2205). These differences might have been indicative of some degree of passivity breakdown perhaps associated with the onset of SCC. However, although the three specimens mentioned previously were more frequently inspected for cracks, no cracks were found. Specimen #1 potential trend was cyclical in nature, with some dips being the low points of potential for the 316L group. Specimen #9 and #15 were the lowest potential specimens of their alloy group, and in the case of specimen #15, well below any other specimen, but after numerous inspections, no sign of cracking was found on either specimen.

Some surface etching was noted on specimen #15, potentially indicative of incipient corrosion in progress, but the amount was not significant enough over the time interval for a concern of failure.

The importance of the Phase 2 results in comparison to the Phase 1 results is that Phase 1 results were obtained not only at much higher temperatures, but the Phase 1 tests did not factor in the effects of high pH (and hydroxides) into the susceptibility to corrosion. While Phase 1 allowed for the prediction of the initiation of SCC over the life span of the alloy, Phase 2 incorporated corrosion-inhibiting factors that would be present in prestressed concrete. While sea water contains many salts, only NaCl was used as it is the most abundant salt in sea water, and would therefore be the salt most likely to reach and build up next to the stainless steel strand. The fact that no alloy experienced SCC while in SPS suggests that high pH can have a significant beneficial effect on the susceptibility of stainless steels to SCC. It is also noted that in the Phase 1 extrapolation, 316L should have SCC initiated after 0.06 years at 40°C (104°F) while at the same temperature 316L showed no signs of SCC in Phase 2 after 0.25 years. This observation suggests that lowering of the temperature was not a significant cause for lack of SCC initiation in Phase 2.

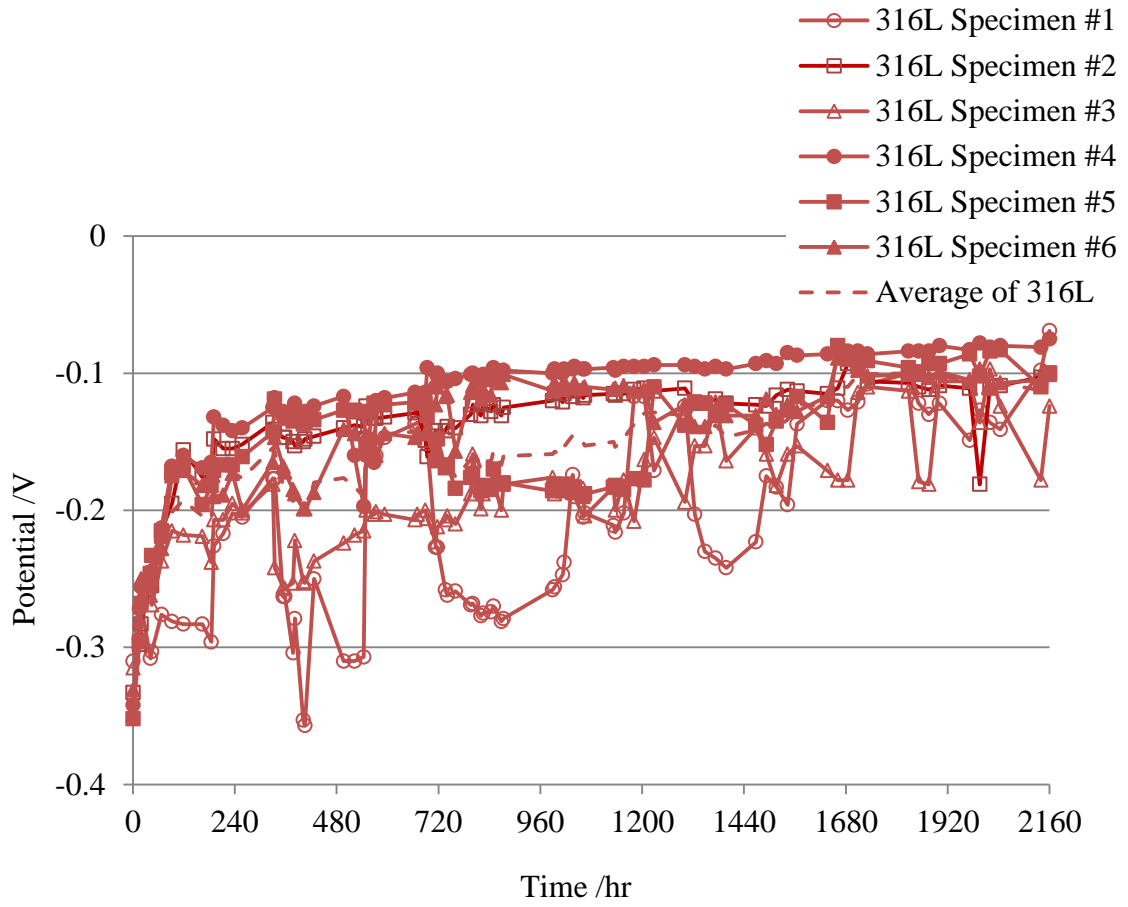


Figure 29 Potential versus Time for 316L Specimens #1 through #6 (SCE versus ATR)

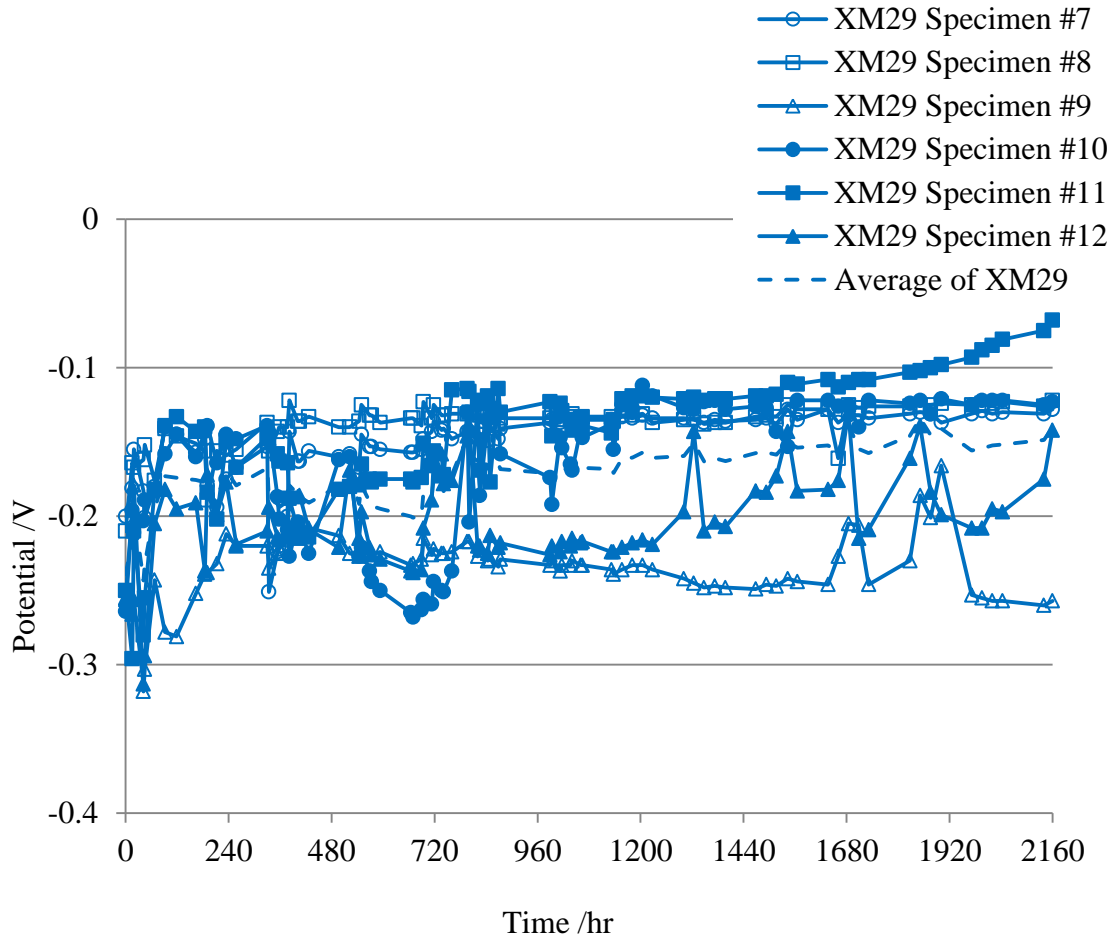


Figure 30 Potential versus Time for XM29 Specimens #7 through #12 (SCE versus ATR)

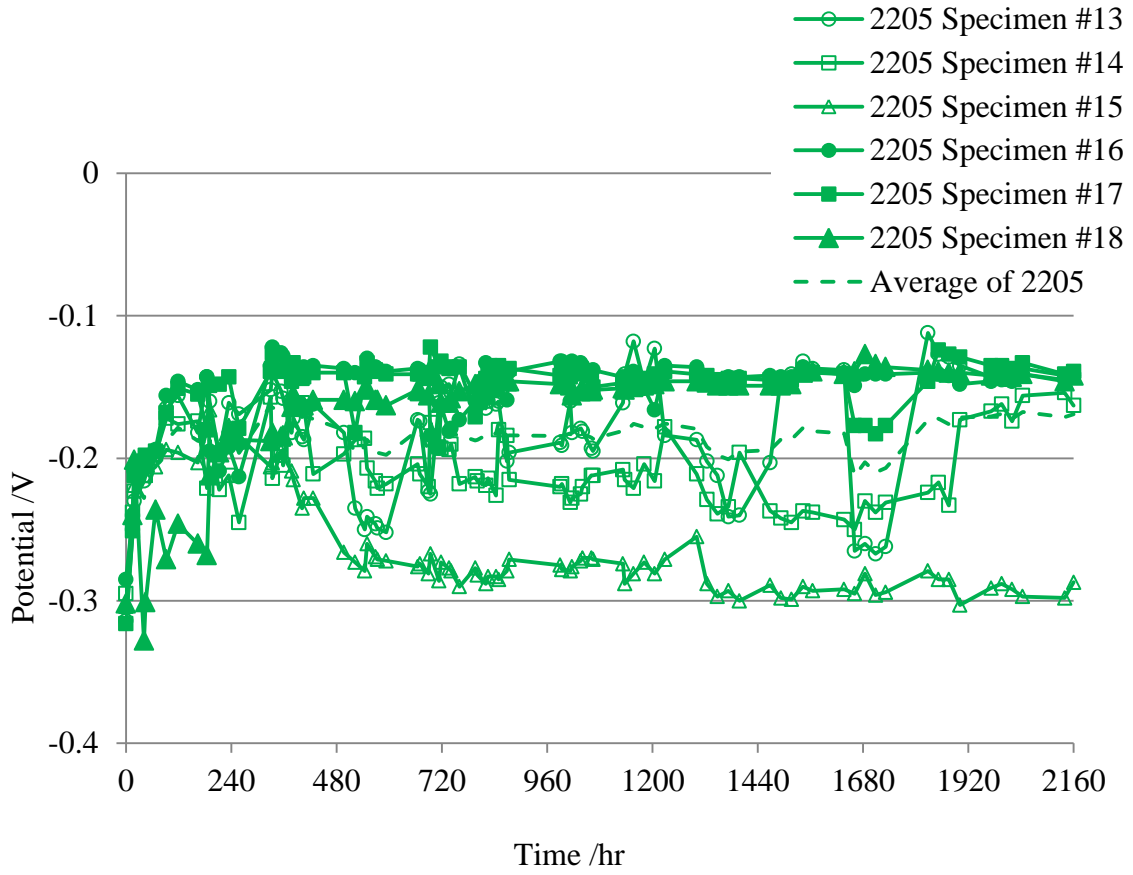


Figure 31 Potential versus Time for 2205 Specimens #13 through #18 (SCE versus ATR)

Chapter 4: Overall Discussion

Within the limited context of the above experiments, XM29 appears to be a promising candidate for further evaluation for use as prestressed strand for concrete construction in marine environments. This observation is derived from the performance of XM29 when evaluated at high temperatures (up to 135°C / 275°F) and high chloride concentrations (>30 wt%) well above those expected in concrete service. Of the three alloys analyzed in this experiment, XM 29 required longer times at each of the three temperatures tested at to have SCC initiated in it than in 316L or 2205 specimens. Also, XM29 did not show indication of SCC while tested for longer periods of time in a more realistic set of conditions (high pH environment of simulated pore solution and 15% chloride concentration at 40°C (104°F)).

The accelerated testing permitted calculation of activation energies (Q) for extrapolation from those results to a time frame of that similar to actual service. Values of Q were 81.3 kJ /mol for XM29 and 71.5 kJ /mol for 316L.

The activation energy found for XM29 yielded a time to crack versus temperature curve projecting no SCC within 82 years (greater than the 75 year service life goal) at the high end of expected near-ambient temperatures.

The alloy 316L showed susceptibility to SCC in a chloride environment even at temperatures as low as 60°C (140°F). SCC was projected to occur in 316L well before a service life of 75 years.

The performance of alloy 2205 was between those of 316L and XM29. At the highest temperature tested (135°C / 275 F), 2205 cracked within 1 hour, just as 316L did. At lower temperatures, its performance was similar to that of XM 29. It showed etching in Phase 2 of the experiment, which did not occur in XM 29, and further testing will be needed to ensure that the etching of 2205 in a high pH condition will not cause SCC to occur.

The two phases of this experiment showed that the effect of chloride on the susceptibility of high-strength stainless steels to SCC is dependent on the compositional makeup of that alloy, and suggest that SCC may affect high-strength stainless steels even at temperatures easily experienced in many marine environments. In these limited tests the performance of XM29 suggested its consideration for further evaluation as a material for prestressed concrete construction. However, this preliminary finding is subject to confirmation by expanded tests in progress where a broader set of service environment conditions is evaluated.

Chapter 5: Conclusions

Based on the results of this research, the following conclusions were reached.

- An approach was devised and implemented for evaluating susceptibility to SCC of candidate high-strength stainless steel alloys under accelerating high temperature and high chloride concentration regimes, while avoiding galvanic prevention artifacts due to corrosion of the test frame.
- As shown in figure 28, extrapolations from the moderate-to-high temperature MgCl_2 test results were made using Arrhenius relationships to project at what nominal time SCC could occur at lower temperatures. The projection for 40°C was in excess of 75 years for XM29, but much shorter for the other two alloys.
- Using information obtained from the accelerated tests, a second experiment (Phase 2) was conducted to evaluate the alloys at temperatures and chloride concentration regimes closer to those experienced in a marine environment, as well as the effects of high pH pore water on the initiation of SCC. The absence of cracking after 2160 hours suggested lower susceptibility to SCC under these conditions.
- In these limited tests, the SCC performance of XM29 was better relative to that of the other two alloys. The issue of potential SCC susceptibility of these materials remains a concern, however. Evaluation should continue in conditions more

closely approaching those for prestressed concrete construction in marine environments.

Chapter 6: Future Work

A list of future work that should be done based on the results and conclusions of this research are shown below.

- Longer runs on 2205 at 60°C (140°F) to find a time where SCC occurs so a more accurate Time versus Temperature graph can be made for 2205 as well as the calculation of the activation energy.
- Other stainless steel alloys as well as other materials, such as composites, could be tested for SCC susceptibility using the methodology of the first phase of the experiment.
- Continued experimentation similar to Phase 2 testing, should be conducted. In particular, tests at higher temperatures and in less alkaline pH conditions should be conducted to determine if the alloy ranking obtained here is still supported.

References

- 1 “Corrosion Forecasting for 75-Year Durability Design of Reinforced Concrete”, A. Sagüés, S.C. Kranc, F. Presuel-Moreno, D. Rey, A. Torres-Acosta, L. Yao, Florida Department of Transportation Final Report BA502 (located at <http://www.dot.state.fl.us>), December 2001.
- 2 “Design of Prestressed Concrete Structures”, T.Y. Lin, N. H. Burns, 3rd Edition, John Wiley & Sons, Hoboken, NJ, 1955.
- 3 “CIP 35 – Testing Compressive Strength of Concrete”, Published by NRMCA Silver Spring, MD, , 2003.
- 4 “Tensile Strength as a Design Parameter”, Industrial & Materials Technologies Programme (Brite-EuRam III), EuroLightCon Document BE96-3942/R32, Contract BRPR-CT97-0381, Project BE96-3942, June 2000.
- 5 “A Critical Literature Review of High-Performance Corrosion Reinforcement in Concrete Bridge Applications”, W. H. Hartt, R. G. Powers, V. Leroux, and D. K. Lysogorski, Federal Highway Administration Report, FHWA-HRT-04-093 (located at <http://www.fhwa.dot.gov>), July 2004.
- 6 “Product Data Bulletin - Hot-Rolled Steel”, Product Catalog Sheet from AK Steel Corporation, 2007.
- 7 “ASM Specialty Handbook Stainless Steels”, J.R. Davis, ASM International, Materials Park, OH, December 1994.
- 8 Steel prices for strand were obtained from the Carpenter Technology website at [http://www.cartech.com](http://www.carttech.com).
- 9 “Corrosion Engineering”, M. Fontana and N. Greene, 2nd Edition, McGraw-Hill, New York, NY, 1986.
- 10 “Modeling the Effects of Corrosion on the Lifetime of Extended Reinforced Concrete Structures”, A. Sagüés, Corrosion, Volume 59 No. 10, Pages 854-866, October 2003.

- 11 "Introduction to Corrosion Prevention and Control", P.J. Gellings, Delft University Press, Fairfax, VA, 1985.
- 12 "Ambient-Temperature Stress-Corrosion Cracking of Austenitic Stainless Steel in Swimming Pools", J. Oldfield and B. Todd, Nickel Development Institute Series No. 14 015, December 1990.
- 13 "Effects of Relative Humidity and Chloride type on Stainless-Steel Room-Temperature Atmospheric Corrosion Cracking" S. Shoji and N. Ohnaka, Corrosion Engineering, Volume 38 No. 2, Pages 111-119, 1989.
- 14 "Solving Some Key Failure Analysis Problems using Advanced Methods for Materials Testing" S. Shipilov, Engineering Failure Analysis, Volume 14, Pages 1550-1573, January 2007.
- 15 "Materials Science and Engineering, An Introduction", W. Callister, 5th Edition, John Wiley & Sons, Hoboken, NJ, 2000.
- 16 "Principles and Prevention of Corrosion", D. Jones, 2nd Edition, Prentice Hall, NJ, 1996.
- 17 "Stress-Corrosion Cracking Materials Performance and Evaluation", R. H. Jones, ASM International, January 1992.
- 18 "Stress Corrosion Cracking Mechanism of Prestressing Steels in Bicarbonate Solutions" C. Andrade, J. Sanchez and J. Fulla, Advances in Construction Materials, Part V, Pages 397-404, 2007.
- 19 "Stress Corrosion Failure of Large Diameter Pressure Pipelines of Prestressed Concrete" A. Valiente, Engineering Failure Analysis, Volume 8, Pages 245-261, 2001.
- 20 "SCC of Stainless Steel under Evaporative Conditions" H. Andersen, P. Amvig, W. Wasielewska, L. Wegrelius, and C. Wolfe, Avesta Sheffield R&D ACOM No 3-98, 1998.
- 21 "Marine Atmospheric SCC of Unsensitized Stainless Steel Rock Climbing Protection" A. Sjong and L. Eiselstein, Journal of Failure Analysis and Prevention, Volume 8, Pages 410-418, August 2008.
- 22 "Pier in Progresso, Mexico Inspection Report, Evaluation of Stainless Steel Reinforcement", Requested by Arminox Steel, Job No. 990022, March 1999.

- 23 "Low-Temperature Stress Corrosion Cracking of Stainless Steels in the Atmosphere in the Presence of Chloride Deposits" T. Prosek, A. Iversen, C. Taxen, and D. Thierry, *Corrosion*, Volume 65 No. 2, Pages 105-117, February 2009.
- 24 "Susceptibility of Duplex Stainless Steels to Corrosion and Stress Corrosion Cracking in Pulping Liquors", A. Bhattacharya, J. Mahmood, P. M. Singh, Conference Paper from 2007 Engineering, Pulping, and Environmental Conference (located at www.tappi.org).
- 25 "Manganese Effects on Repassivation Kinetics and SCC Susceptibility of High Mn-N Austenitic Stainless Steel Alloys", I. Toor, K. Jin Park, and H. Kwon, *Journal of the Electrochemical Society*, Volume 154, Pages C494-C499, July 2007.
- 26 "Effect of High Mn on SCC Behavior of an Austenitic Stainless Steel in 42% Boiling MgCl₂ Solution" A. Devasenapathi and M. Asawa, *Journal of Materials Science Letters*, Volume 16, Pages 1363-1365, 1997.
- 27 "Some Fundamental Aspects of Thermally Activated Processes involved in Stress Corrosion Cracking in High Temperature Aqueous Environments", Z. Lu, Y. Takeda, and T. Shoji, *Journal of Nuclear Materials*, Volume 383, Pages 92-96, 2008.
- 28 "The Effect of Test Temperature on SCC Behavior of Austenitic Stainless Steels in Boiling Saturated Magnesium Chloride Solution" O. M, Alyousif and R. Nishimura, *Corrosion Science*, Volume 48, Pages 4283-4293, May 2006.
- 29 "High-Strength Stainless Steels for Corrosion Mitigation in Prestressed Concrete: Development and Evaluation", R. Moser, A Dissertation at Georgia Institute of Technology, August 2011.
- 30 "Fastener Tech - the Nuts and Bolts of It", B. Ansell, *Xtreme Off Road Magazine* Issue 1, 2005.
- 31 "Relative Humidity Temperature Relationships of Some Saturated Salt Solutions in the Temperature Range of 0°C to 50°C" A. Wexler and S. Hasegawa, *J. Research NBS* 53: (19), 1954. The basic data from the reference was used up to 50°C and then a compilation with other data sources along with extrapolation was done to create the data used from the PDF file located at [_HYPERLINK "http://www.omega.com/temperature/Z/pdf/z103.pdf" http://www.omega.com/temperature/Z/pdf/z103.pdf](http://www.omega.com/temperature/Z/pdf/z103.pdf).
- 32 "Standard Handbook for Mechanical Engineers", T. Baumeister and Lionel Marks, 7th Edition, McGraw-Hill, New York, NY, 1958.
- 33 "Handbook of Chemistry and Physics", Robert C. Weast, 54th Edition, Published by CRC Press, Boca Raton, FL, 1973-1974.

- 34 "Exploratory Assessment of Corrosion Behavior of Stainless Steel Clad Rebar" F. Cui and A. Sagüés, *Corrosion*, Volume 62 No. 9, Pages 822-838, September 2006.
- 35 "Elements of Materials Science and Engineering", Lawrence Van Vlack, 6th Edition, Addison-Wesley Publication Co, Boston, MA, 1975.
- 36 "Humidity Control in the Laboratory using Salt Solutions-a Review" J. F. Young, *Journal of Applied Chemistry*, Volume 17, Pages 241-245, September 1967.
- 37 "Corrosion of the Strand-Anchorage System in Post-Tensioned Grouted Assemblies" H. Wang, A. Sagüés, and R. Powers, NACE 2005 Conference Paper 05266, 2005.
- 38 "Susceptibility of Alloy 22 to Environmentally Assisted Cracking in Yucca Mountain Relevant Environments", J. Estill, K. King, D. Fix, D. Spurlock, G. Hust, Steven Gordon, D. McCright and R.L. Rebak, NACE 2002 Conference Paper 02535, 2002.
- 39 "Stress Corrosion Cracking Test Methods", A. Sedriks, Volume 1, Published by National Association of Corrosion Engineers (NACE) Houston, Texas, 1990.
- 40 "Selection of Metallic Materials for Stress Corrosion Cracking Resistance in Sodium Chloride Environments" National Aeronautics and Space Administration Technical Standard NASA-STD-P025, August 27, 2001.
- 41 "Corrosion Induced Failure Mechanisms", U. Nurnberger, Otto-Graf-Institut, University of Stuttgart Germany, 2006.
- 42 "Effects of Alloy Chemistry, Cold Work, and Water Chemistry on Corrosion Fatigue and Stress Corrosion Cracking of Nickel Alloys and Welds", O.K. Chopra, W.K. Soppet, and W.J. Shack, U.S. Nuclear Regulatory Commission and Argonne National Laboratory, NUREG/CR-6721 and ANL-01/07, March 2001.

About the Author

Joseph Fernandez was born in Perth Amboy, New Jersey in 1978 and raised in Saint Petersburg, Florida most of his life. He earned a B.S. Degree in Nuclear Engineering from Purdue University in 2000. He worked at Sciencetech Inc. as a Probabilistic Risk Analysis consultant for about a year working on such nuclear power plants as Cook, Clinton, and San Onofre Nuclear Power Plant. He then moved out west to consult for General Electric as a Probabilistic Risk Analyst for their Nuclear Power Plant project known as Lungmen Unit 4 in Taiwan.